Appl. Phys. B 87, 565–593 (2007)
DOI: 10.1007/s00340-007-2643-5

Applied Physics B
Lasers and Optics

Invited paper

J. VANIER[1,✉]
C. MANDACHE[2]

The passive optically pumped Rb frequency standard: the laser approach

[1] Département de Physique, Université de Montréal, Montréal QC, Canada, H3C 3J7
[2] INFLPR, Atomistilor, PO. Box MG-36, 76900 Bucharest, Romania

Received: 31 January 2007
Published online: 17 May 2007 • © Springer-Verlag 2007

ABSTRACT This paper outlines the progress made during the last few decades in the implementation of a frequency standard using the optical-microwave double resonance technique and laser optical pumping in a sealed cell containing an alkali atom vapor in a microwave cavity. An analysis is presented based on a three-level model, describing the basic phenomena taking place in that approach. The expected frequency stability is calculated. The various frequency shifts taking place are described and their importance is evaluated. Several laser systems generally used in this context are described as well as the various techniques for stabilizing them. The results obtained by several research groups are outlined, compared to the analysis, and evaluated in the context of the implementation of a practical frequency standard. Conclusions are drawn relative to the future of a realistic implementation of such a laser pumped frequency standard.

PACS 06.30.Ft; 32.10.Fn; 32.30.Bv; 32.70.Jz; 32.80.Wu

1 Introduction

Since their early laboratory realizations in the late 1950s [1–3], atomic frequency standards using optical pumping of alkali atoms [4] and the so-called double resonance technique, optical-microwave interaction, have been the subject of continuous development. Major efforts have been dedicated to the improvement of characteristics such as frequency stability, reliability, and to the reduction of power consumption, volume and weight.

Most of the developments of this field have made use of the isotope ^{87}Rb. This is due to the several advantages associated with the use of that isotope, in particular its ground state hyperfine frequency (6.835 GHz) that can be easily synthesized from readily available quartz oscillators, as well as other practical properties such as temperature of operation and availability of pure isotopes. Another advantage of ^{87}Rb resides in the smaller number of ground state Zeeman sublevels due to its smaller nuclear spin ($I = 3/2$) as compared to ^{85}Rb ($I = 5/2$), and Cs ($I = 7/2$). This characteristics has the advantage of increasing the population of the pair of levels involved in the clock transition and consequently providing a larger signal. However, one of the most important advantages of using ^{87}Rb has been the fortuitous coincidence of an optical spectral line of both isotopes ^{85}Rb and ^{87}Rb. This coincidence allows rather efficient optical filtering of a ^{87}Rb spectral lamp by a cell containing ^{85}Rb [5]. When exploited in a proper experimental arrangement, this fortuitous coincidence allows the inversion of population by optical pumping of the ground state hyperfine levels of ^{87}Rb contained as a vapor in a cell with an appropriate inert buffer gas. The buffer gas maintains the atoms in place during the interaction with the microwave field and prevents ground state relaxation by collisions of the atoms with the cell walls [1, 6–8]. In such a case, the cell becomes transparent to the incident radiation. When the cell is exposed to microwave radiation at the hyperfine frequency, transitions tend to equalize the ground state population among the two hyperfine levels. Under this excitation the cell becomes partially opaque to the incident radiation and the phenomenon provides a means of detecting the coincidence between the applied microwave radiation and the hyperfine resonance. The resulting signal is used as a reference to lock in frequency the microwave generator that provides the excitation, resulting in the implementation of a frequency standard or atomic clock. The approach is generally called the "double-resonance technique". The technique just described, called the separated filter approach, has been used to a great extent in frequency standards implemented up to now. Another approach, in which the hyperfine filtering is done directly in the absorption cell, by means of a proper mixture of the isotopes, called the integrated filter approach, has also been developed [9] and provides a simpler means for implementing a frequency standard of this type with excellent characteristics [10]. It is worth mentioning that the separated filter approach is rather efficient for optical pumping. When used in the proper experimental arrangement, it creates a population inversion that provides sufficient gain to allow the implementation of a maser oscillator [11, 12].

The use of other alkali atoms such as Cs has been hindered by the lack of proper isotopic filtering. Although an hyperfine filter using a strong magnetic field to shift optical lines has been successful [13], the technique has remained at the laboratory level due mainly to the required cumbersome experimental arrangement and the resulting size of the device [14].

Early in their development, lasers have been suggested as sources of radiation for optical pumping. The evident advantage is the narrowness of the radiation spectrum, which

✉ E-mail: jac.vanier@sympatico.ca

provides efficient optical pumping without the need of filtering. However, sources at the proper wavelength were not readily available until the advent of the solid state diode laser, except for the case of the cumbersome dye laser. In the 1970s, solid state diode lasers became available at wavelengths corresponding to the resonant D_1 and D_2 spectral lines of some alkali atoms [15, 16]. With a power of several mW and spectral width less than 100 MHz, they provided sources of radiation that appeared suitable to replace the spectral lamps used up to that time. The field has been the subject of a large number of studies. In general, implementations have fulfilled expectations, but sometime at the expense of more complexity than expected. Furthermore, the predicted frequency stability often was not reached unless special arrangements were implemented in order to compensate for the extra noise introduced by the laser itself. At the time of writing, sealed cell frequency standards using laser optical pumping and the double-resonance technique have been the subject of a large number of laboratory implementations but are not available yet commercially.

It is important to realize that the double-resonant technique considered here does not make use directly of the coherent property of the laser radiation, but mainly of its narrow spectrum. It is, thus, totally different from the coherent population trapping approach (CPT), reviewed in a previous article [17], and whose operation is based on the coherence of the laser radiation field. The present approach is often called intensity optical pumping (IOP) since its effectiveness relies primarily on the laser intensity [18].

The present paper examines the state of the art in the use of a diode laser in the implementation of an optically pumped sealed cell frequency standard. First, an analysis is made of the atomic physics involved and results relative to signal contrast, line width, and frequency shifts are summarized. A review is made of the experimental results obtained in several laboratories in the implementation of a standard using such an approach. A review of the type of laser sources presently available with their characteristics is also made. Various laser frequency stabilization schemes are examined. Finally, conclusions are drawn on the present status of implementation of such a standard with a look at the future.

2 The optically pumped closed-cell Rb atomic clock

2.1 *Basic principles*

In this section, the general principles of operation of a double resonance optically pumped sealed-cell atomic frequency standard are reviewed. The classical approach used in this field for the implementation of such a frequency standard has been based on the use of the ^{87}Rb isotope and is shown in Fig. 1 [19].

In this setup, as mentioned earlier, light emitted by the spectral lamp excited at about 100 MHz is filtered by a cell containing ^{85}Rb. The fortuitous coincidence of the atomic transitions is such that the spectral line corresponding to the transition $S_{1/2}$, $F = 2 \leftrightarrow P$ emitted by the lamp is partly absorbed by this so-called hyperfine filter placed in the path of the radiation as illustrated. Consequently, as shown in inset 1 of Fig. 1, the radiation reaching the resonance cell consists mainly of the spectral line $S_{1/2}$, $F = 1 \leftrightarrow P$. This radiation causes optical pumping altering the population of the two hyperfine levels and making the cell transparent to the incident radiation. The cell is placed in a microwave cavity resonant at the ground state hyperfine frequency of ^{87}Rb. When energy is fed to the cavity at that frequency, the field created within the cell causes transitions between the two hyperfine energy levels and tend to equalize their population. The cell becomes absorbing again at the transition $S_{1/2}$, $F = 1 \leftrightarrow P$.

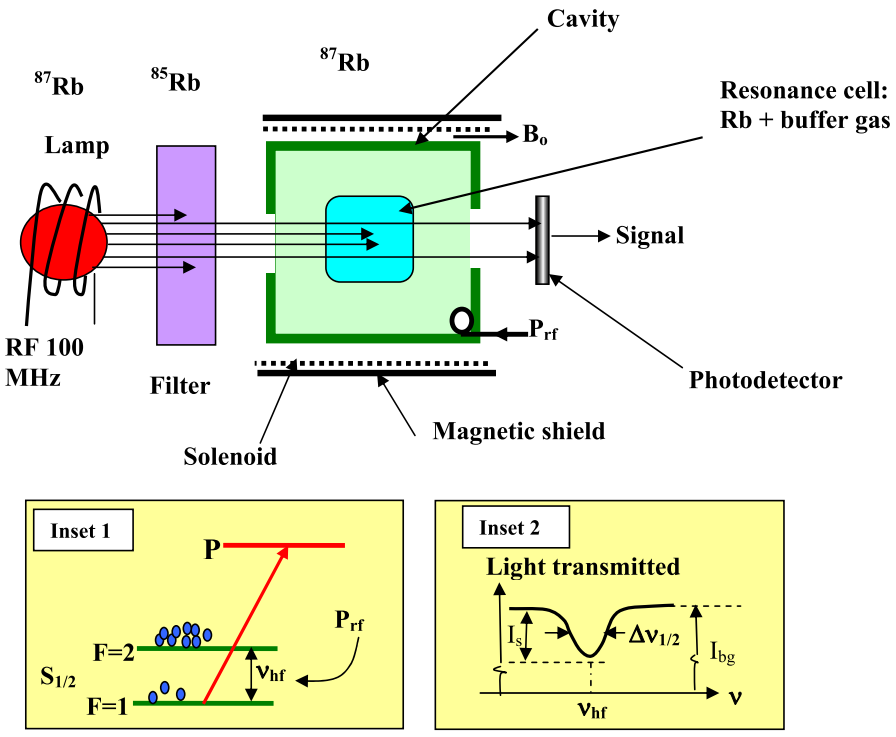

FIGURE 1 General approach used in the implementation of a double resonance classical ^{87}Rb frequency standard using a ^{87}Rb spectral lamp and a ^{85}Rb filter. The two *insets* illustrate respectively the dynamics of the double-resonance technique (optical-microwave) and the resonance signal imbedded in the transmitted light reaching the photodetector as a function of microwave frequency

The phenomenon observed is illustrated in Fig. 1 as inset 2. A resonance line is observed in the light reaching the photodetector, and its characteristics reflect the properties of the ground state hyperfine transition: the line has a frequency relatively independent of the environment and is rather narrow, its width being determined largely by relaxation taking place in the $S_{1/2}$ ground state. An inert buffer gas is used in the cell in order to prevent relaxation by collisions of the atoms with the walls of the containing cell. In the case that the microwave is applied as a traveling wave without a cavity, Doppler broadening is avoided with the buffer gas through Dicke effect. In the present analysis we will assume the presence of a cavity and of a standing wave. The relaxation rate is mainly controlled by spin exchange interaction, collisions with the buffer gas atoms, diffusion to the container walls, and interaction of the atoms with the pumping light itself. In this approach, it is possible to obtain line widths of a few hundred Hz giving a line Q of the order of 10^7 to 10^8. In the arrangement shown in Fig. 1, the resonance cell and cavity are placed inside a solenoid creating a small magnetic field required to provide a quantization axis, and inside a magnetic shield preventing fluctuations in the environmental magnetic field from affecting the atoms resonant frequency.

2.2 *Frequency stability*

For implementing a frequency standard, the microwave generator used to feed the cavity and excite the hyperfine transition of ^{87}Rb is locked by means of a frequency control loop to the frequency of the resonance line as observed at the photodetector. In that approach, the microwave generator frequency is modulated at a low frequency of the order of one hundred Hz to a depth of a fraction of the hyperfine resonance line width. The signal at the photodetector, processed by means of synchronous detection, approximates the derivative of the resonance line and provides a frequency discrimination pattern. This signal can be used to lock in frequency the microwave generator to the center of the resonance line. In practice the microwave generator consists of a quartz crystal oscillator synthesized numerically to the desired frequency ν_{hf}.

A straightforward linear circuit analysis shows that the frequency stability of the hyperfine resonance line is transferred to the quartz oscillator [20] and the resulting frequency stability of the system in the time domain is given by [19, 21]

$$\sigma(\tau) = \frac{KN}{\nu_0 I_{\mathrm{bg}} q} \tau^{-1/2} , \tag{1}$$

where N is the noise spectral density observed at the photo detector originating from all sources, I_{bg} is the current developed in the photodetector by the background radiation and τ is the averaging time. K is a factor that depends on the modulation wave form and is of the order of 0.2. The parameter "q" is the so-called quality factor defined as the ratio of the contrast C of the resonance line to its line width $\Delta\nu_{1/2}$. Using the illustration in inset 2 in Fig. 1, we have

$$C = \frac{I_{\mathrm{s}}}{I_{\mathrm{bg}}} \tag{2}$$

and

$$q = \frac{C}{\Delta\nu_{1/2}} . \tag{3}$$

In the approach using a spectral lamp, the resulting pumping radiation consists of both D_1 and D_2 components and contains several hyperfine lines.

The width of these lines are of the order of 1 GHz and, although hyperfine filtering reduces the intensity of the lines corresponding to the transitions $S_{1/2}$, $F = 2$ to $P_{1/2}$ and $P_{3/2}$, the radiation reaching the detector is intense and causes so-called shot noise whose spectral density is given by

$$N^2 = 2eI_{\mathrm{bg}} , \tag{4}$$

where e is the charge of the electron. In such a case, $\sigma(\tau)$ becomes proportional to the square root of I_{bg}. In standard operation, I_{bg} is large and this type of noise is generally predominant, well above thermal noise at the detector. Furthermore, the contrast of the hyperfine resonance line is small (a few tenths of a percent) due to the presence of optical lines that do not contribute to optical pumping or to the signal, and due also to the background radiation originating from the noble gas used to initiate and maintain the lamp plasma excitation. Assuming a line width of the order of 250–500 Hz, the quality factor, as defined by (3), is calculated to be $\sim 10^{-5}$. In practice, using a spectral lamp as illustrated in Fig. 1, the background light intensity may correspond to a current of $\sim 100\,\mu$A, and the shot noise limited frequency stability is calculated to be approximately 0.5 to 1×10^{-11}. Instruments using either the integrated or the separated filter approach have a frequency stability in general agreement with this calculation, smaller units showing frequency instabilities above $10^{-11}\,\tau^{-1/2}$.

The above considerations show that in the case of shot noise, frequency stability is controlled by three parameters: line width, contrast and background current. Consequently, a reduction in background radiation should result in better frequency stability in the shot noise limit. This consideration and possible simplification in design and construction have created an interest in the use of solid state diode lasers instead of spectral lamps for implementing that type of clock. This is due to the fact that the laser spectrum is very narrow, < 100 MHz, resulting in a more efficient optical pumping, leading to less background radiation and higher contrast of the hyperfine resonance line. In practice, as will be described below, a contrast larger than 10% is observed with laser optical pumping, due essentially to a reduction of the background current by about two orders of magnitude.

3 Laser optical pumping

3.1 *Choice of atom*

The choice of the atom for the implementation of a frequency standard of the type discussed here is rather limited due to various environmental considerations such as temperature of operation, power consumption, and the obvious condition that a solid state laser with the appropriate wavelength be readily available at reasonable cost. This reduces essentially the choice to the isotopes ^{87}Rb, ^{85}Rb and ^{133}Cs. The required wavelengths are tabulated in Table 1 [19]:

	ν_{hf}	D_1 (in air)	D_2 (in air)
^{87}Rb	6.835 ... GHz	794.76 nm	780.02 nm
^{85}Rb	3.035 ... GHz	794.76 nm	780.02 nm
^{133}Cs	9.192 ... GHz	894.35 nm	852.11 nm

TABLE 1 Alkali metal isotopes and required wavelengths for optical pumping

The availability of lasers at these wavelengths and their characteristics will be discussed below. We will assume that such lasers are available and will make an analysis for the double-resonance technique described above, but using a laser for optical pumping rather than a spectral lamp.

3.2 *Basic theory*

The analysis is developed for the case of ^{87}Rb optically pumped with a laser tuned to the $S_{1/2} - P_{1/2}$ transition (D_1 radiation). The energy levels involved in the optical pumping process are shown in Fig. 2.

A typical experimental arrangement is shown in Fig. 3. The system includes two servo loops, one for locking the laser wavelength to the optical absorption line selected, and one for locking the frequency of the microwave generator to the hyperfine resonance line. When switch SW1 is closed, the arrangement acts as a frequency standard, while when it is open the arrangement may be used as a spectrometer for studying the response of the resonance cell to either double resonance (optical-microwave), or laser excitation alone.

As in the classical approach using a spectral lamp, a buffer gas is used for preventing relaxation of Rb atoms on the wall of the cell. This buffer gas is generally a mixture of a noble gas with nitrogen as a constituent. The purpose of the mixture is to reduce considerably the dependence of the ^{87}Rb resonance frequency on temperature as will be explained below. On the other hand, nitrogen is used specifically for quenching fluorescence radiation through collisions with Rb atoms in

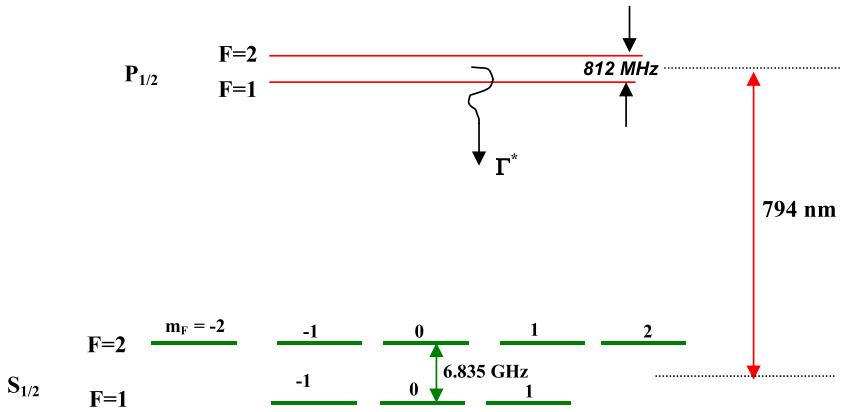

FIGURE 2 Ground state and first excited state energy manifolds of ^{87}Rb

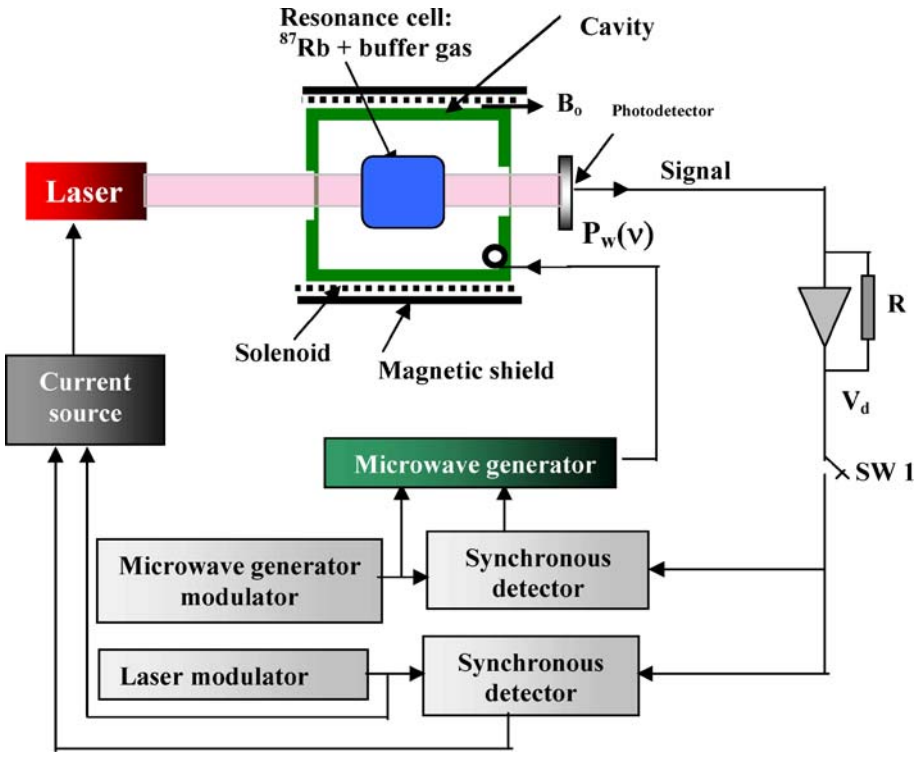

FIGURE 3 Typical experimental setup used in the study of laser optical pumping for the implementation of a frequency standard with a sealed cell. The system can be used as a spectrometer (switch SW1 opened), or a frequency standard (switch SW1 closed)

the excited state [22]. This process prevents optical pumping that would take place by means of scattered radiation, which would act as an added relaxation mechanism. The nitrogen–Rb atom collisions cause mixing of the $P_{1/2} - P_{3/2}$ states as well as decay of the Rb atoms from those states, resulting in a broadening of the optical resonance line at 794 nm. On the other hand, noble gas–Rb collisions introduce a certain degree of dephasing within the optical transition, which also causes optical broadening. In the analysis, it would seem natural to separate the two effects, excited state decay and dephasing. However, due to the complexity of the processes involved and the uncertainty on their relative importance in line broadening, we will assume that the resulting combined effect is a broadening of the excited state and we will simply associate this effect to a decay of the excited state. The broadening due to buffer gas collisions, as measured from absorption spectra, is about 20 MHz per Torr, added to the Doppler broadening, which is 530 MHz at a normal temperature of operation ($\sim 60\,^{\circ}$C). At a buffer gas pressure of 20 Torr, the optical line width is thus of the order of 930 MHz. For all practical purposes it is Lorentzian. This point was examined in [17] where the absorption spectrum under various light polarization conditions was examined. It should be noted that the spontaneous emission rate broadening is of the order of 5 MHz and is very small compared to the effect of buffer gas collisions. Consequently, we characterize the excited state decay rate by the parameter Γ^*. We evaluate its size from the observed line width to be about $2–5 \times 10^9\ \mathrm{s}^{-1}$ at the pressures considered in the present analysis.

The selection rules of this decay are not known. Consequently, it is assumed that the decay takes place to all Zeeman sublevels of the ground state with equal probability. With the buffer gas broadening considered, the splitting of the excited state is barely resolved. In practice, the laser is normally tuned to the transition $S_{1/2}$, $F = 1$ to $P_{1/2}$, $F = 1$. Consequently, in view of these characteristics, that is equal decay rate to all levels of the ground state and partially resolved hyperfine structure of the excited state, we use a simple three-level model in the analysis. The overlapping transition $S_{1/2}$, $F = 1$ to $P_{1/2}$, $F = 2$, does not affect much the analysis in the three-level model aside from altering slightly the calculated pumping rate and causing an added light shift. The alteration of the pumping rate can be taken care of by adjusting the calculated pumping rate while the light shift can be taken care of in a perturbation approach.

It should be mentioned that the use of unpolarized radiation prevents any population trapping in an end Zeeman level as is introduced in the case of optical pumping with circular polarization [23]. On the other hand, the use of linear polarization could have an effect on the final distribution of population among the ground state Zeeman levels. However, in view of the remarks made above in connection with random decay from the excited state, it is assumed that the radiation is unpolarized and that all Zeeman levels within one hyperfine level are equally populated.

Relaxation within the ground state takes place at rates γ_1 and γ_2 for the populations and the coherence respectively. Contributions to these rates originate from various interactions as follows:

$$\gamma_1 = \gamma_{1\mathrm{bg}} + \gamma_{1\mathrm{w}} + \gamma_{1\mathrm{se}} \tag{5}$$

$$\gamma_2 = \gamma_{2\mathrm{bg}} + \gamma_{2\mathrm{w}} + \gamma_{2\mathrm{se}} \tag{6}$$

where $\gamma_{1\mathrm{bg}} + \gamma_{1\mathrm{w}}$ are caused by collisions with the buffer gas and diffusion to the cell walls and $\gamma_{1\mathrm{se}}$ is the spin-exchange collision relaxation rate. Similar definitions apply to γ_2. In practice γ_1 and γ_2 are almost equal. They can be calculated from detailed expressions given in [19].

Following this discussion we thus assume that the Rb ensemble can be represented by the three-level model shown in Fig. 4.

In this model the laser may be tuned to either of the ground state hyperfine levels. In the analysis the laser spectrum is assumed to be broad enough to cover the splitting by the applied magnetic field of all ground state Zeeman levels within one hyperfine level but much narrower than the ground state hyperfine splitting. We are interested in the resonance signal of the field independent transition $F = 1$, $m_F = 0$ to $F = 2$, $m_F = 0$. This may be taken into account at the end of the analysis by considerations on the number of atoms contributing to the resonance signal as compared to those contributing to the total light absorption (essentially two out of eight atoms in proportion to the number of Zeeman levels).

The system "radiation fields–atomic ensemble" is analyzed in the density matrix formalism [24, 25]. The dynamical behavior of the matrix elements representing the population of the energy levels, ϱ_{ii}, and the coherence, ϱ_{ij}, existing in the system, is obtained from Liouville's equation:

$$\frac{\mathrm{d}}{\mathrm{d}t}\varrho_{jk} = (\mathrm{i}\hbar)^{-1} \sum_i (H_{ji}\varrho_{ik} - \varrho_{ji}H_{ik}) \,, \tag{7}$$

where H is the interaction Hamiltonian of the various fields applied, in occurrence the laser and the microwave radiation fields. In the analysis, we use an approach similar to that used in [19]. However, we keep all terms corresponding to the laser

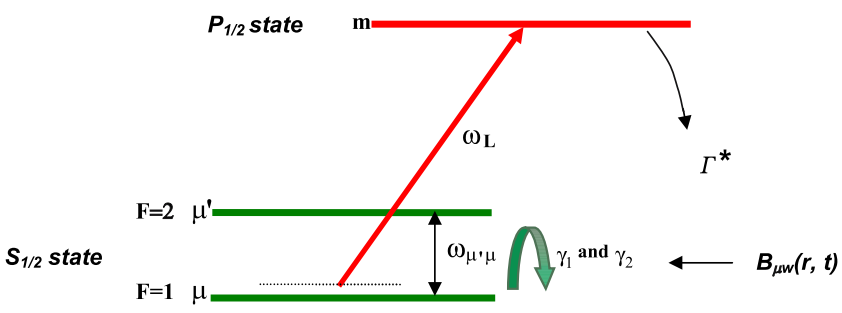

FIGURE 4 Three-level model used in the present analysis for double resonance in ^{87}Rb. In practice the laser is tuned close to either of the two transitions from μ or μ' to m

interaction with both levels of the ground state. The approach allows the possibility of examining the effect of pumping from one level or the other and leads to a more realistic evaluation of the light shift.

The optical radiation field is written as

$$\boldsymbol{E}(\omega_{\mathrm{L}}, t, z) = E_{o\mathrm{L}}\boldsymbol{e}_{\lambda}\cos(\omega_{\mathrm{L}}t + \boldsymbol{k}\cdot\boldsymbol{r})\,, \tag{8}$$

where $E_{o\mathrm{L}}$ is the laser radiation field amplitude, $\boldsymbol{e}_{\lambda}$ the polarization vector, ω_{L} the angular frequency and $\boldsymbol{k}$ is the propagation vector. We define the optical Rabi angular frequencies $\Omega_{\mathrm{L}m\mu'}$ and $\Omega_{\mathrm{L}m\mu}$ as:

$$\Omega_{\mathrm{L}m\mu'} = (E_{o\mathrm{L}}/\hbar)\left\langle\mu'\left|e\boldsymbol{r}\cdot\boldsymbol{e}_{\lambda}\right|m\right\rangle = (E_{o\mathrm{L}}/\hbar)d_{\mu' m}\,, \tag{9}$$

$$\Omega_{\mathrm{L}m\mu} = (E_{o\mathrm{L}}/\hbar)\left\langle\mu\left|e\boldsymbol{r}\cdot\boldsymbol{e}_{\lambda}\right|m\right\rangle = (E_{o\mathrm{L}}/\hbar)d_{\mu m}\,, \tag{10}$$

where $\hbar$ is Plank's constant over 2π. The terms within brackets are the so-called dipole matrix elements d_{im} of the two possible transitions. We assume that a microwave field is present in the cavity and has the form

$$\boldsymbol{B}_{\mu w}(r, t) = \boldsymbol{z}B_1\cos(\omega_{\mathrm{M}}t)\,, \tag{11}$$

where B_1 is the microwave field amplitude and ω_{M} is its angular frequency. The Rabi angular frequency associated with this field is defined as

$$b(r) = \mu_B\mu_0 H_z(r)/\hbar\,. \tag{12}$$

where μ_B is Bohr magneton and μ_0 is the permeability of free space. For simplifying the calculation, we assume that the microwave field is homogeneous over the resonance cell. This assumption has no fundamental consequences on the calculation. We will examine this point further below.

We evaluate the various terms in (7) and obtain a set of rate equations for the populations and the coherence of the atomic ensemble. Relaxation in the ground state and decay from the excited state are introduced in a phenomenological way. In view of the low laser light intensities used and the large decay rate from the excited P state, the fractional population of the excited state is always very small. This is taken into account in the equations for the ground state populations, by assuming that the total population is the sum of the populations of the two ground state energy levels.

$$\frac{\mathrm{d}\varrho_{\mu'\mu'}}{\mathrm{d}t} = -b\,\mathrm{Im}\,\varrho_{\mu\mu'}\mathrm{e}^{-\mathrm{i}\omega_{\mathrm{M}}t} + \Omega_{\mathrm{L}m\mu'}\,\mathrm{Im}\,\varrho_{\mu' m}\mathrm{e}^{-\mathrm{i}\omega_{\mathrm{L}}t} + \frac{\Gamma^*}{2}\varrho_{mm} - \gamma_1(\varrho_{\mu'\mu'} - 1/2) \tag{13}$$

$$\frac{\mathrm{d}\varrho_{mm}}{\mathrm{d}t} = -\Omega_{\mathrm{L}m\mu}\,\mathrm{Im}\,\varrho_{\mu m}\mathrm{e}^{-\mathrm{i}\omega_{\mathrm{L}}t} - \Omega_{\mathrm{L}m\mu'}\,\mathrm{Im}\,\varrho_{\mu' m}\mathrm{e}^{-\mathrm{i}\omega_{\mathrm{L}}t} - \Gamma^*\varrho_{mm} \tag{14}$$

$$\frac{\mathrm{d}\varrho_{\mu' m}}{\mathrm{d}t} = \mathrm{i}\omega_{m\mu'}\varrho_{\mu' m} + \mathrm{i}\frac{\Omega_{\mathrm{L}\mu' m}}{2}\mathrm{e}^{\mathrm{i}\omega_{\mathrm{L}}t}(\varrho_{mm} - \varrho_{\mu'\mu'}) + \mathrm{i}\frac{b}{2}\mathrm{e}^{-\mathrm{i}\omega_{\mathrm{M}}t}\varrho_{\mu m} - \mathrm{i}\frac{\Omega_{\mathrm{L}\mu m}}{2}\mathrm{e}^{\mathrm{i}\omega_{\mathrm{L}}t}\varrho_{\mu'\mu} - \frac{\Gamma^*}{2}\varrho_{\mu' m} \tag{15}$$

$$\frac{\mathrm{d}\varrho_{\mu\mu}}{\mathrm{d}t} = +b\,\mathrm{Im}\,\varrho_{\mu\mu'}\mathrm{e}^{-\mathrm{i}\omega_{\mathrm{M}}t} + \Omega_{\mathrm{L}m\mu}\,\mathrm{Im}\,\varrho_{\mu m}\mathrm{e}^{-\mathrm{i}\omega_{\mathrm{L}}t} + \frac{\Gamma^*}{2}\varrho_{mm} - \gamma_1(\varrho_{\mu\mu} - 1/2) \tag{16}$$

$$\frac{\mathrm{d}\varrho_{\mu m}}{\mathrm{d}t} = \mathrm{i}\omega_{m\mu}\varrho_{\mu m} + \mathrm{i}\frac{\Omega_{\mathrm{L}\mu m}}{2}\mathrm{e}^{\mathrm{i}\omega_{\mathrm{L}}t}(\varrho_{mm} - \varrho_{\mu\mu}) + \mathrm{i}\frac{b}{2}\mathrm{e}^{\mathrm{i}\omega_{\mathrm{M}}t}\varrho_{\mu' m} - \mathrm{i}\frac{\Omega_{\mathrm{L}\mu' m}}{2}\mathrm{e}^{\mathrm{i}\omega_{\mathrm{L}}t}\varrho_{\mu\mu'} - \frac{\Gamma^*}{2}\varrho_{\mu m} \tag{17}$$

$$\frac{\mathrm{d}\varrho_{\mu\mu'}}{\mathrm{d}t} = \mathrm{i}\omega_{\mu'\mu}\varrho_{\mu\mu'} + \frac{\mathrm{i}b}{2}\mathrm{e}^{\mathrm{i}\omega_{\mathrm{M}}t}(\varrho_{\mu'\mu'} - \varrho_{\mu\mu}) + \mathrm{i}\frac{\Omega_{\mathrm{L}\mu m}}{2}\mathrm{e}^{\mathrm{i}\omega_{\mathrm{L}}t}\varrho_{m\mu'} - \mathrm{i}\frac{\Omega_{\mathrm{L}m\mu'}}{2}\mathrm{e}^{-\mathrm{i}\omega_{\mathrm{L}}t}\varrho_{\mu m} - \gamma_2\varrho_{\mu\mu'} \tag{18}$$

$$\varrho_{\mu'\mu'} + \varrho_{\mu\mu} = 1\,. \tag{19}$$

These equations contain all the information on the response of the atomic ensemble to the two electromagnetic fields applied, taking into account the various relaxation mechanisms that are present in the ensemble.

The physical parameter looked for is the intensity of the radiation at the exit of the resonance cell as detected at the photodetector shown in Fig. 3. It is measured as a voltage V_{d} at the output of the trans-impedance amplifier. V_{d} is proportional to the current developed in the photodetector and is proportional to the light intensity or the radiation power transmitted. Authors have taken various approaches in evaluating theoretically the effect of absorption on the transmitted radiation [19, 26, 27]. All these approaches are equivalent as is shown in Appendix A. We choose the method developed in [27, 28]. The technique is straightforward and gives rise to a first order differential equation for the field amplitude at any point within the cell as a function of parameters that can be calculated from a solution of the set of (13) to (19) above.

The local electric field E is a function of distance z within the cell and is related to the electric polarization P at that point by the equation [19]

$$\frac{\partial^2\boldsymbol{E}}{\partial z^2} - \varepsilon_0\mu_0\frac{\partial^2\boldsymbol{E}}{\partial t^2} = \mu_0\frac{\partial^2\boldsymbol{P}}{\partial t^2}\,. \tag{20}$$

where ε_0 is the vacuum dielectric constant. The Rabi frequencies for both optical transitions and the electric field are related through (9) and (10). We assume that the laser is tuned close to the transition μ to m and only atoms in level μ contribute to the absorption due to the fact that the laser spectrum is much narrower than the hyperfine splitting. However, the effect of the other transitions is kept in the equations since, even though it is off resonance, it causes a light shift through virtual transitions. Equation (20) can be transformed readily into [27]:

$$\frac{\partial\Omega_{\mathrm{L}\mu m}}{\partial z} = \alpha\,\mathrm{Im}\,\delta_{\mu m}\,, \tag{21}$$

where $\delta_{\mu m}$ is the complex amplitude of the optical coherence to be defined below and

$$\alpha = \left(\frac{\omega_{m\mu}}{c\varepsilon_0\hbar}d_{\mu m}^2\right)n\,, \quad [\mathrm{m}^{-1}\mathrm{s}^{-1}] \tag{22}$$

is the absorption coefficient, with c being the speed of light, ε_0 the permeability of free space and n the atomic density.

The problem, thus, consists of evaluating $\delta_{\mu m}$ from (13) to (19), and integrating (21) for obtaining the Rabi frequency

proportional to the electric field at any point within the resonance cell and particularly at the exit, with $z = L$. From the information obtained it is then possible in principle to draw conclusions regarding background radiation, contrast, and line width as a function of several parameters such as light intensity, Rb density, and microwave power.

In the following analysis, we assume that the intensity of the laser radiation is constant in the radial direction. This experimental restriction will be discussed below.

3.3 *Contrast, line width, and light shift*

We assume that the coherences excited by the laser and the microwave radiation are given by the expressions:

$$\varrho_{\mu\mu'}(z,t) = \delta_{\mu\mu'}(z,t)\mathrm{e}^{\mathrm{i}\omega_{\mathrm{M}}t} \tag{23}$$

$$\varrho_{\mu m}(z,t) = \delta_{\mu m}(z,t)\mathrm{e}^{\mathrm{i}\omega_{\mathrm{L}}t} + \varepsilon_{\mu m}(z,t)\mathrm{e}^{\mathrm{i}(\omega_{\mathrm{L}}+\omega_{\mathrm{M}})t} \tag{24}$$

$$\varrho_{\mu' m}(z,t) = \delta_{\mu' m}(z,t)\mathrm{e}^{\mathrm{i}\omega_{\mathrm{L}}t} + \varepsilon_{\mu' m}(z,t)\mathrm{e}^{\mathrm{i}(\omega_{\mathrm{L}}-\omega_{\mathrm{M}})t}\,. \tag{25}$$

The calculation of $\delta_{\mu m}$ required in (21) involves some algebra but is straightforward, as described in [19], where a similar calculation is made for a simpler case. In the analysis, we assume the following values for various parameters, values that are typical of experimental conditions:

$$\gamma_1 \sim \gamma_2 \sim 500\ \mathrm{s}^{-1}\,, \quad \Gamma^* = 2\times 10^9\ \mathrm{s}^{-1}\,.$$

The Rabi frequencies are variable but are of the order of

$$b \sim 1 \text{ to } 5\times 10^3\ \mathrm{s}^{-1}$$

$$\Omega_{\mathrm{L}\mu m} = \Omega_{\mathrm{L}\mu' m} \sim 1 \text{ to } 5\times 10^6\ \mathrm{s}^{-1}\,.$$

In view of the various decay and relaxation rates, the values just chosen make all optical coherences very small relative to the ground state coherence. Furthermore, at laser intensities used in the present application, the fractional population of the excited state ϱ_{mm} is of the order of 10^{-6}. These considerations make possible a number of approximations valid over a broad range of microwave and optical Rabi frequencies. We find that the ground state coherence created by the microwave field is given by

$$\delta_{\mu\mu'} = \mathrm{i}\frac{(b/2)\left(\gamma_2 + \frac{\Gamma_{p\mu}+\Gamma_{p\mu'}}{2}\right)}{\left(\gamma_2 + \frac{\Gamma_{p\mu}+\Gamma_{p\mu'}}{2}\right)^2 + (\omega_{\mathrm{M}} + (\Delta\omega_{l\mu} - \Delta\omega_{l\mu'}) - \omega_{\mu'\mu})^2}\Delta + \frac{(b/2)(\omega_{\mathrm{M}} + (\Delta\omega_{l\mu} - \Delta\omega_{l\mu'}) - \omega_{\mu'\mu})}{\left(\gamma_2 + \frac{\Gamma_{p\mu}+\Gamma_{p\mu'}}{2}\right)^2 + (\omega_{\mathrm{M}} + (\Delta\omega_{l\mu} - \Delta\omega_{l\mu'}) - \omega_{\mu'\mu})^2}\Delta\,, \tag{26}$$

where Δ, defined as the population difference between the two ground state levels, is given by

$$\Delta = \frac{(1/2)(\Gamma_{p\mu} - \Gamma_{p\mu'})}{\left(\gamma_2 + \frac{\Gamma_{p\mu}+\Gamma_{p\mu'}}{2}\right) + \frac{b^2\left(\gamma_2 + \frac{\Gamma_{p\mu}+\Gamma_{p\mu'}}{2}\right)}{\left(\gamma_2 + \frac{\Gamma_{p\mu}+\Gamma_{p\mu'}}{2}\right)^2 + (\omega_{\mathrm{M}} + (\Delta\omega_{l\mu} - \Delta\omega_{l\mu'}) - \omega_{\mu'\mu})^2}}\,. \tag{27}$$

On the other hand, the optical coherence $\delta_{\mu m}$ is a solution of the equation:

$$\delta_{\mu m} = -\mathrm{i}\frac{\Omega_{\mathrm{L}\mu m}/2}{\left(\frac{\Gamma^*}{2} + \mathrm{i}(\omega_{\mathrm{L}} - \omega_{m\mu})\right)}\varrho_{\mu\mu} + \frac{(b/2)^2}{\left(\frac{\Gamma^*}{2} + \mathrm{i}(\omega_{\mathrm{L}} - \omega_{m\mu})\right)\left(\frac{\Gamma^*}{2} + \mathrm{i}(\omega_{\mathrm{L}} - \omega_{\mathrm{M}} - \omega_{m\mu'})\right)}\delta_{\mu m} - \frac{(\Omega_{\mathrm{L}\mu m}/2)(b/2)}{\left(\frac{\Gamma^*}{2} + \mathrm{i}(\omega_{\mathrm{L}} - \omega_{m\mu})\right)\left(\frac{\Gamma^*}{2} + \mathrm{i}(\omega_{\mathrm{L}} - \omega_{\mathrm{M}} - \omega_{m\mu'})\right)}\delta_{\mu' m} \tag{28}$$

A similar expression is obtained for $\delta_{\mu' m}$ (see Appendix B). In these expressions the following definitions have been introduced:

$$\Gamma_{p\mu} = \frac{|\Omega_{\mathrm{L}\mu m}/2|^2\Gamma^*}{(\Gamma^*/2)^2 + (\omega_{\mathrm{L}} - \omega_{\mathrm{M}} - \omega_{m\mu'})^2}\,,$$

pumping rate from level μ (29)

$$\Gamma_{p\mu'} = \frac{|\Omega_{\mathrm{L}\mu' m}/2|^2\Gamma^*}{(\Gamma^*/2)^2 + (\omega_{\mathrm{L}} + \omega_{\mathrm{M}} - \omega_{m\mu})^2}\,,$$

pumping rate from level μ' (30)

$$\Delta\omega_{l\mu} = \frac{|\Omega_{\mathrm{L}\mu m}/2|^2(\omega_{\mathrm{L}} - \omega_{\mathrm{M}} - \omega_{m\mu'})}{(\Gamma^*/2)^2 + (\omega_{\mathrm{L}} - \omega_{\mathrm{M}} - \omega_{m\mu'})^2}\,,$$

light shift from level μ (31)

$$\Delta\omega_{l\mu'} = \frac{|\Omega_{\mathrm{L}\mu' m}/2|^2(\omega_{\mathrm{L}} - \omega_{\mathrm{M}} - \omega_{m\mu})}{(\Gamma^*/2)^2 + (\omega_{\mathrm{L}} - \omega_{\mathrm{M}} - \omega_{m\mu})^2}\,,$$

light shift from level μ' (32)

We take note that

$$\omega_{\mathrm{L}} - \omega_{\mathrm{M}} - \omega_{m\mu'} = \omega_{\mathrm{L}} - \omega_{m\mu} \tag{33}$$

$$\omega_{\mathrm{L}} + \omega_{\mathrm{M}} - \omega_{m\mu} = \omega_{\mathrm{L}} - \omega_{m\mu'} \tag{34}$$

The above expressions for the light shift can of course be derived in several other ways, for example, by means of the operator formalism developed by Happer and Mather [29] or still by considering optical pumping as a relaxation process [30]. In the present case, using a laser as a pumping source, the keeping of the optical coherence simplifies the evaluation of the light shift. and of light transmitted by means of (21), even though the final mechanism is intensity optical pumping.

With the values assumed for the Rabi frequencies, several approximations can be made. Since we have assumed "b" to be of the order of 10^3, $\Omega_{\mathrm{L}\mu m}$ of the order of 10^6, and Γ^* of the order of 10^9, the two last terms on the right hand side of (28) are negligible. We are, thus, left with

$$\delta_{\mu m} = -\mathrm{i}\frac{\Omega_{\mathrm{L}\mu m}/2}{\left(\frac{\Gamma^*}{2} + \mathrm{i}(\omega_{\mathrm{L}} - \omega_{m\mu})\right)}\varrho_{\mu\mu}\,. \tag{35}$$

This essentially implies that the transition from μ to m is driven mainly by the direct interaction of the laser and not by feedback from the other transition μ' to m through the coherence $\delta_{\mu\mu'}$.

The value of $\varrho_{\mu\mu}$ is obtained from the set of equations, (13) to (19). Within the approximations just made, we finally

obtain

$$\varrho_{\mu\mu} = \left(\frac{1}{2}\right)\frac{\gamma_1 + \Gamma_{p\mu'}}{\gamma_1'} + \frac{1}{\gamma_1'}\frac{S}{S+1} \times \frac{(1/4)\left(\Gamma_{p\mu} - \Gamma_{p\mu'}\right)}{1 + \left(\omega_{\mathrm{M}} - \omega'_{\mu'\mu}\right)^2/(\gamma_2'(S+1))}\,, \tag{36}$$

where

$$\gamma_1' = \gamma_1 + (1/2)(\Gamma_{p\mu} + \Gamma_{p\mu'}) \tag{37}$$

$$\gamma_2' = \gamma_2 + (1/2)(\Gamma_{p\mu} + \Gamma_{p\mu'}) \tag{38}$$

$$\omega'_{\mu'\mu} = -(\Delta\omega_{l\mu} - \Delta\omega_{l\mu'}) + \omega_{\mu'\mu} \tag{39}$$

and S is the saturation factor defined as

$$S = \frac{b^2}{\gamma_1'\gamma_2'}\,. \tag{40}$$

We note that (36) is identical to the result obtained in [19] for a calculation made in a phenomenological way in terms of pumping rates only. In the present case, a complete analysis in terms of the coherence introduced by the laser radiation provides exact expressions for the light shift and pumping rates and gives insight on the relative importance of various coherences introduced by the laser and the microwave radiation.

The first term of (36) gives the equilibrium population under the effect of optical pumping alone, assuming the laser tuned close to the transition from the lower ground state level μ to the excited level m. The second term gives the resonance signal under the influence of the applied microwave radiation represented by the Rabi angular frequency "b". An equation similar to that of (36) can be obtained for the laser tuned close to the transition from the upper ground state level μ' to the excited level m.

Equation (36) is valid locally. Since the laser radiation is absorbed in the cell, the pumping light intensity decreases with the distance z traveled within the cell. Consequently, the pumping rates Γ_{pi} are functions of distance within the resonance cell. In the case that the laser is tuned exactly to the transition μ to m, $\Gamma_{p\mu'}$ is very small compared to $\Gamma_{p\mu}$ and can be neglected. $\Gamma_{p\mu}$ is then given by (29), which becomes

$$\Gamma_{p\mu} = \frac{|\Omega_{\mathrm{L}\mu m}|^2}{\Gamma^*}\,, \tag{41}$$

where $\Omega_{\mathrm{L}\mu m}$ is a function of z. Equation (35) is replaced in (21) and at optical resonance we have:

$$\frac{\mathrm{d}\Omega_{\mathrm{L}\mu m}}{\mathrm{d}z} = -\alpha\frac{\Omega_{\mathrm{L}\mu\, m}}{\Gamma^*}\varrho_{\mu\mu} \tag{42}$$

with $\varrho_{\mu\mu}$ given by (36). This system cannot be solved analytically. It is solved numerically and the results are used to obtain signal amplitude and contrast as a function of various parameters. On the other hand, the full line width at half maximum is obtained from (36) and is given by

$$\Delta\nu_{1/2} = \frac{1}{\pi}\gamma_2'(S+1)^{1/2}\,. \tag{43}$$

Consequently, $\Delta\nu_{1/2}$ can be calculated at the exit of the cell by proper evaluation of the pumping rates and saturation factor. Following the discussion of Sect. 2.2 on frequency stability, it appears that an important parameter is the quality factor q, proportional to the contrast. We, thus, extend the above analysis by making a numerical evaluation of the contrast that appears possible within the hypothesis made. This numerical calculation was done for several values of the absorption coefficient α as well as for several microwave field intensities in the cavity as a function of light intensity or pumping rate at the entrance of the cell. The length of the cell was assumed to be 2 cm. In the calculation, the contrast is obtained from (2) in terms of the Rabi frequency:

$$C = \left|\frac{\left(\Omega^2_{\mathrm{L}\mu m}(z=L,\omega=\omega_{\mu'\mu}) - \Omega^2_{\mathrm{L}\mu m}(z=L,\omega_{\mathrm{M}}-\omega_{\mu'\mu}=100\,000)\right)}{\Omega^2_{\mathrm{L}\mu m}(z=L,\omega_{\mathrm{M}}-\omega_{\mu'\mu}=100\,000)}\right| \tag{44}$$

The frequency difference imposed, $\omega_{\mathrm{M}} - \omega_{\mu'\mu} = 100\,000$, guarantees that for the background radiation the Rabi frequency is evaluated well outside microwave resonance.

Typical results are shown in Figs. 5 and 6 for the contrast and the line width under various conditions representative of typical experimental situations. In those figures, the microwave Rabi frequency is fixed at a value of $1.41 \times 10^3\ \mathrm{s}^{-1}$.

Similar calculations were done for a fixed absorption coefficient $\alpha = 2 \times 10^{11}\ \mathrm{m}^{-1}\mathrm{s}^{-1}$ but as a function of the microwave Rabi frequency with the pumping rate Γ_{p} as a parameter. The results are shown in Figs. 7 and 8.

Various conclusions can be drawn immediately from those figures. First, due to low spurious background radiation, the contrast can be large and reach a value of the order of 10 to 20% at high Rb densities (large α). This is more that an order of magnitude larger than with a lamp. As expected, the line width increases with light intensity, although non-linearly at low values of Γ_{p}. This is due to the non-linear nature of optical absorption at high Rb densities. The homogeneous model would give a line width that increases linearly with light intensity at all values of Γ_{p}.

On the other hand, it is found that the contrast increases with microwave power applied, but tends to a limit. This saturation behavior is due to the fact that above a certain value of the microwave intensity, the population of the two ground state energy levels is equalized and the absorption coefficient becomes constant above a certain value of the Rabi frequency b. On the other hand, it is observed that the microwave excitation broadens the line considerably as made explicit in Fig. 8 and, although the contrast may become large, there is obviously no increase of the quality factor q as defined by (3) above. The line width increases linearly with the microwave field at high values of the Rabi frequency.

The other phenomenon that affects the operation of the frequency standard is the light shift given by (31) and (32). This shift is large and affects the characteristics of the laser pumped frequency standard in an important manner. It displaces the position of the ground state energy levels relative to each other, and consequently changes the transition frequency in an important way [30–32]. The analysis made above, however, is approximate in the sense that it considers only three energy levels. The complete calculation of this shift for a prac-

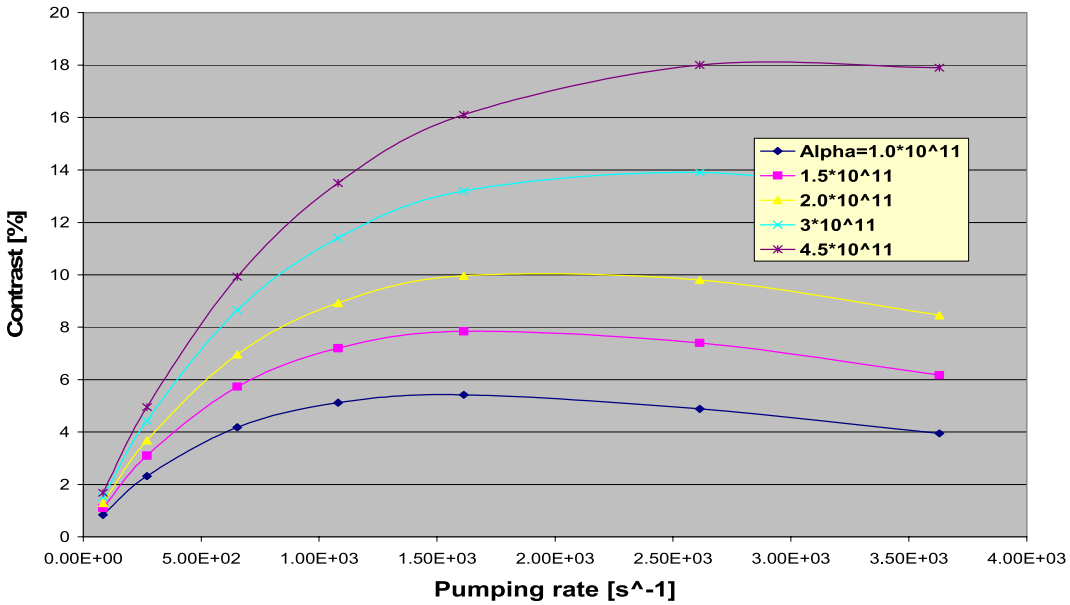

FIGURE 5 (Theory) Contrast calculated as a function of pumping rate for various values of the absorption coefficient. The microwave Rabi frequency, b, is assumed to be 1.41×10^3 s^{-1}. The points in the graphs originate from the software used in the calculation and help in identifying the various curves

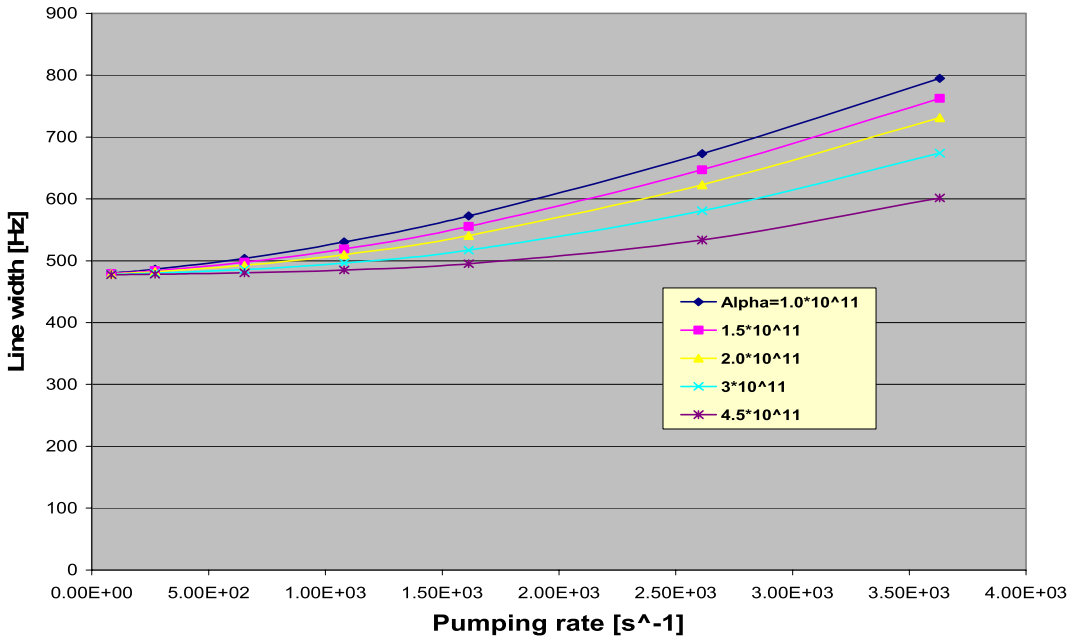

FIGURE 6 (Theory) Line width calculated as a function of pumping rate for various values of the absorption coefficient. The microwave Rabi frequency is assumed to be 1.41×10^3 s^{-1}

tical situation would be rather complex. First, the P states of the ^{87}Rb atom is formed of several hyperfine energy levels. On one hand, the $P_{3/2}$ state consists of 4 levels separated by 266, 153, and 70 MHz respectively. The average wavelength for the transition to the ground state is 780 nm. On the other hand, the $P_{1/2}$ state consists of two hyperfine levels separated by 812 MHz and this transition has an average wavelength of 795 nm. Lasers are available for both wavelengths generally known as D_2 and D_1 respectively. The transition probability from the ground levels to each of these excited hyperfine levels varies according to rules connected to angular momentum matrix algebra (Clebsch–Gordan coefficients) and the absorption line is broadened by buffer gas collisions. Furthermore, the presence of Doppler broadening forces an averaging over velocities by means of a Maxwell distribution. Finally, radial intensity inhomogeneities of the laser beam, to be discussed below, alter the pumping rates across the beam and consequently alter the shift itself. The shift is also altered within the cell, the radiation being submitted to absorption along the propagation path.

Measurement results to be examined below are generally reported for very diverse experimental conditions regarding Rb density (temperature), buffer gas pressure, type of lasers, spectral width, and beam diameter. In view of all these considerations it is very difficult to develop an analysis that would cover experimental data at large. Furthermore, the purpose

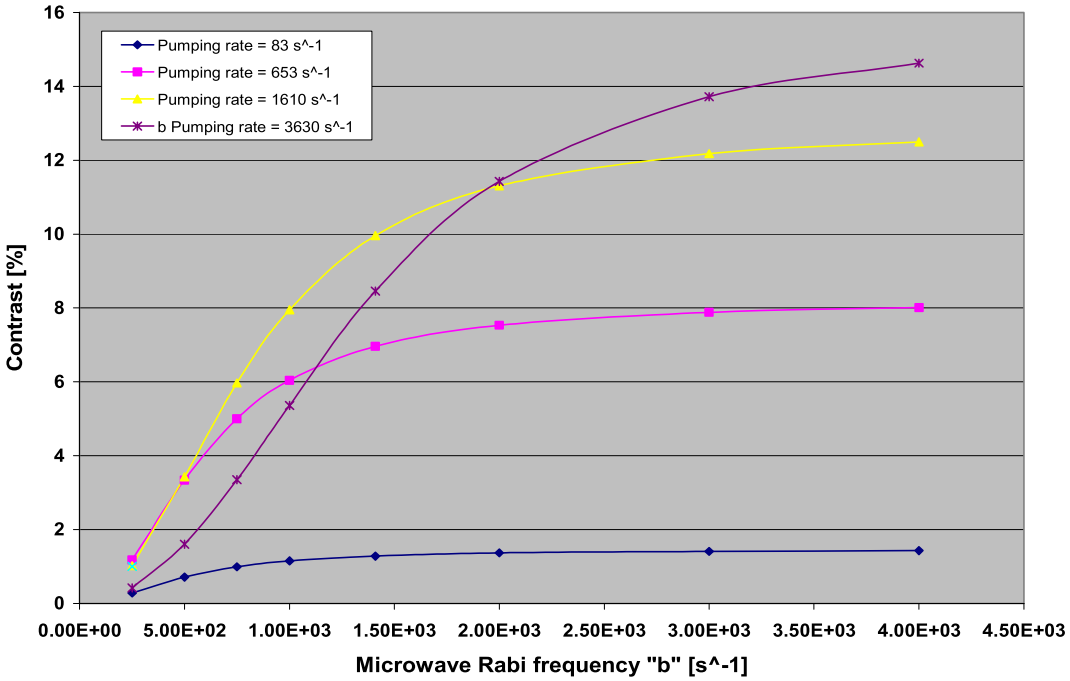

FIGURE 7 (Theory) Contrast as a function of the microwave Rabi frequency for four pumping rates. The absorption coefficient is set at $\alpha = 2 \times 10^{11}\ \mathrm{m}^{-1}\mathrm{s}^{-1}$

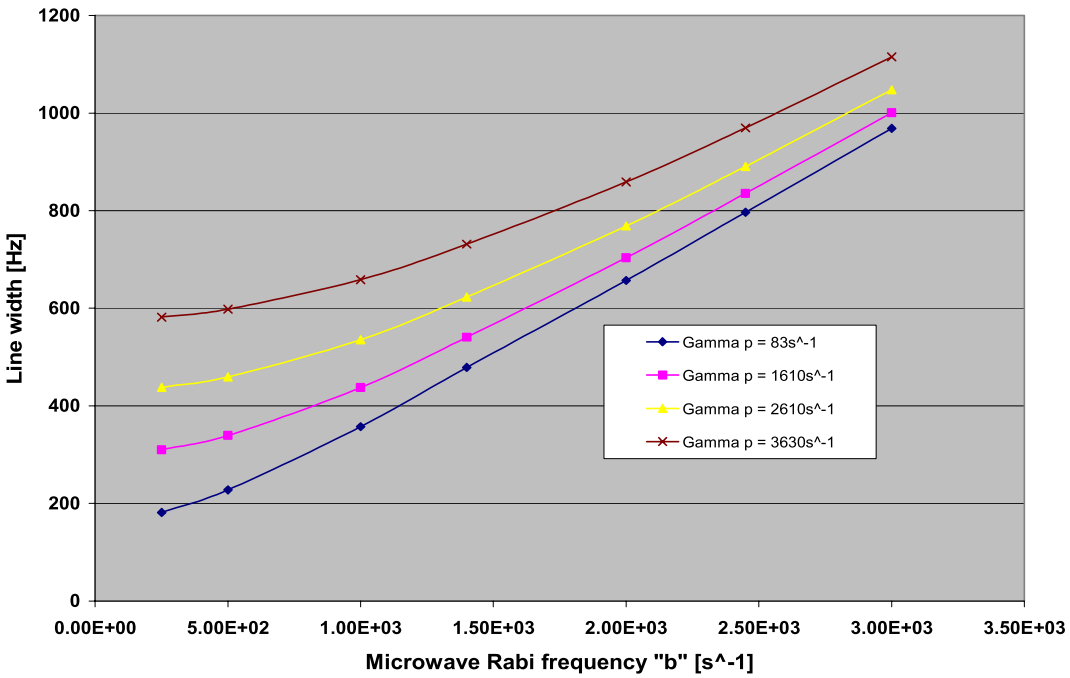

FIGURE 8 (Theory) Line width as a function of the microwave Rabi frequency for four values of the pumping rate Γ_p. The absorption coefficient has been set at $\alpha = 2 \times 10^{11}\ \mathrm{m}^{-1}\mathrm{s}^{-1}$

of the present article is to review the subject in the context of application to the implementation of a frequency standard. Consequently, the goal is not to verify in detail the exactness of the theory developed by means of comparison to experimental data, but to identify controlling parameters of the light shift and review proposed practical approaches and directions for reducing it. The analysis developed above should then be considered as a guide in the search for improvements rather than a full explanation of experimental observations.

We have, thus, evaluated approximately the light shift for a specific simple situation. We have used the three-level model for a given buffer gas pressure that broadens the optical absorption line to ~ 1 GHz, including Doppler effect. This corresponds to a gas, such as nitrogen, at a pressure of about 3 kPa (25 Torr). In view of the important homogeneous broadening that takes place, it is expected that optical pumping is effective for all velocities. At that pressure, the shape of the optical absorption becomes approximately Lorentzian masking the

Gaussian shape produced by Doppler broadening (530 MHz at 60 °C). Consequently we adjust the value of Γ^* in (31) and (32) to give the width of the absorption line that is observed in practice (~ 1 GHz). This value is $6.28 \times 10^9\ s^{-1}$. The calculation is, thus, made without averaging over velocities assuming then that all velocities are pumped due to the buffer gas homogeneous broadening. This approach would be less exact at low buffer gas pressures, since the line shape is a so-called Voigt profile originating from the convolution of a Lorentz with a Gaussian line. However, it appears to be a valid approximation in view of the many other effects that take place in the cell due to such causes as inhomogeneous pumping across the laser beam coupled to microwave saturation effects. In this context, it does not appear that a more exact approach is justified at this time. This approach has also been used in the past to calculate the effect of optical pumping on the shape of absorption lines leading to very satisfying results [17].

The line broadening is thus assumed homogeneous and the calculation is made for three values of the pumping rate, $\Gamma_p = 2$, 3 and $4 \times 10^3\ s^{-1}$, corresponding to values in Fig. 6 that produce visible resonance line broadening. Values of the optical Rabi frequency, $\Omega_{L\mu m}$, are calculated from these by means of (29) or (30), providing absolute values of the light shift. The results of that calculation are shown in Fig. 9. As can be observed readily, the light shift in a laser pumped frequency standard is expected to be very important, being in the range of parts in 10^9 to 10^8. In a practical standard, the laser frequency and intensity, thus, need to be well stabilized in order to achieve frequency stability in the 10^{-13}, as realized in existing standards using spectral lamps as pumping sources.

The theoretical results just presented regarding pumping rates, contrast, line width and light shift are similar to those obtained by Camparo and Frueholz [33] and by Mileti [26, 34] in a different mathematical context where the laser was essentially treated as a narrow optical pumping spectral source without coherence. In those calculations the pumping rates are introduced in a phenomenological way in the rate equations and the light shift is introduced as a perturbation. In the present case, however, the optical coherence introduced in the system by the laser is carried all through the analysis. This coherence leads to a very useful approach for calculating the absorption coefficient, the residual light intensity, and the double resonance signal amplitude at the exit of the cell, through the solution of a first order differential equation obtained from Maxwell's equations. Furthermore, the present analysis leads directly and in a natural way to expressions for the line width, the light shifts and the pumping rates and connects those results to the analysis concerning frequency stability. The results obtained in the present analysis for the light shift are also similar to those obtained by Mathur et al. using an operator formalism [32].

In the present calculation of the light shift the hyperfine splitting of the excited state is completely neglected. This approach may be valid at high buffer gas pressures in which case the optical absorption lines are broadened and the excited state hyperfine splitting is not observable. In that case, the center of the optical line appears as an average of the individual hyperfine absorption lines. At low pressure, the effect of the individual transitions can be taken care of by a perturbation approach in which the individual effects are added. In practice, however, the effect of the excited state hyperfine structure may be totally masked by various inhomogeneities of the laser beam to be discussed below.

3.4 *Effect of laser beam shape*

The analysis presented above does not take into account the shape of the laser beam and the variation of the optical pumping rate in the radial direction. In general, the laser intensity is characterized by a Gaussian shape as a function of radius. This has important consequences since various regions of the beam effectively lead to different pumping rates. In practice, the photodetector, being large compared to the laser beam diameter, is exposed to the total beam and an average of the light intensity at the exit of the resonance cell is measured. The effect predicted above, in which the signal goes through a maximum versus pumping rate, the so-called "peaking" effect [26], is then masked. This is due to the fact that since different parts of the cell are exposed to different radiation intensities the resulting signal becomes an average over a range of pumping rates. The same remarks apply to the calculation of the line width and the light shift both varying with the radial distance. For this reason, these parameters are found in certain arrangements to be non-linear at high light intensities [35]. Due to the variation of the radiation intensity across the beam radius, the center frequency of the resonance line is also a function of radial coordinate, due to a varying light shift. A measurement of the signal frequency at maximum is

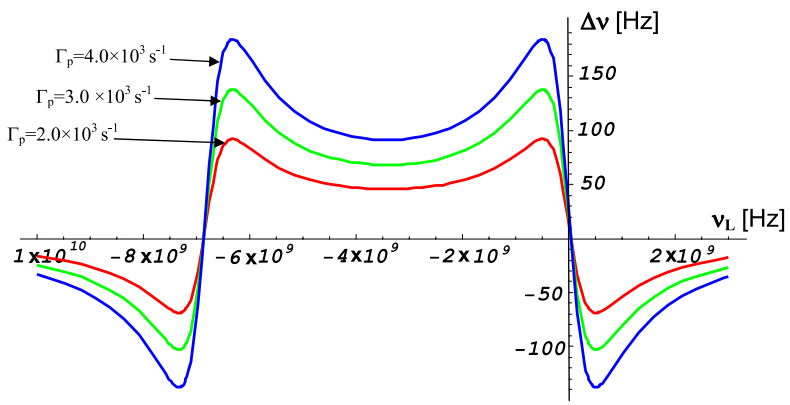

FIGURE 9 (Theory) Light shift expected in ^{87}Rb within the three-level model for three values of the pumping rate corresponding to rates that produce visible broadening (see Figs. 6 and 8). The parameter ν_L used as x axis is the laser frequency and has its origin at the frequency of the transition $S_{1/2}$, $F = 2$ to P

thus an average weighed by factors such as laser beam shape, buffer gas broadening, cavity field geometry, and microwave saturation. The measured light shift depends thus on actual experimental conditions.

It should be mentioned that this effect does not influence appreciably the final conclusion relative to the frequency stability of a frequency standard using a laser as optical pumping source. In practice, in the implementation of a laser pumped frequency standard, one would operate the system at a laser intensity that makes "q" optimum, which is in a region just below the maximum of contrast. The important parameters remain contrast and line width. The light shift has then to be addressed independently and its influence on frequency stability has to be evaluated for each experimental setup.

3.5 *Expectations relative to short term frequency stability*

The results of the analysis just presented provide the background for a calculation of the expected frequency stability of a frequency standard such as one implemented according to Fig. 3. These results make possible the evaluation of the quality factor defined through (3) and consequently provide information to set the optimum point of operation for best frequency stability. For example, assuming an absorption coefficient $\alpha = 2 \times 10^{11}\,\mathrm{m^{-1}s^{-1}}$, corresponding to a cell temperature of about 65 °C, a contrast of 10% is obtained from Fig. 5 at a pumping rate of $2000\,\mathrm{s^{-1}}$ and for a microwave Rabi frequency of $1.41 \times 10^3\,\mathrm{s^{-1}}$. This high contrast is essentially due to the narrow width of the laser spectrum, which is more than an order of magnitude less than the spectral lamp, reducing background radiation. At that pumping rate, the hyperfine resonance line width, according to Figs. 6 and 8, is about 575 Hz. In practice, using a VCSEL in the same situation, a background current of the order of a few microamperes is detected. Taking only shot noise into consideration, one expects the frequency stability to be approximately

$$\sigma(\tau) \cong 10^{-13}\,\tau^{-1/2}$$

as calculated from (1) and (4).

3.6 *Review of experimental results on signal size, line width and frequency stability*

Unfortunately, published experimental data often provide limited information on the conditions realized in practice. Line width is generally provided, but contrast is not a parameter that appears to have drawn attention in past publications. When contrast is reported, usually for a given set of optimum conditions, it is, however, larger than 10%, in qualitative agreement with the general prediction made above [26, 36]. It should be mentioned that in [36], ^{133}Cs was used as the reference alkali atom isotope. However, the system used for implementing a clock is the same as that used with ^{87}Rb and the three-level model developed above applies. The contrast is found to increase to a maximum value with microwave power with a line broadening in qualitative agreement with (43) [26, 36]. The signal amplitude at the photodetector is also often reported as a function of Rb density (cell temperature) and found to decrease at higher temperatures [37, 38]. However, since absorption becomes important at higher temperatures, the background intensity also decreases and no conclusion can be drawn from this information, relative to contrast, quality factor q, and frequency stability, since information on background light intensity is lacking.

On the other hand, the effect of laser intensity variation across the beam on signal intensity was studied in some detail by Mileti [26]. It was made evident through expansion of the laser beam diameter by means of a telescope at the entrance of the cell, making the laser beam more homogeneous, and through the use of annular masks placed in front of the photodetector, hiding part of the laser beam.

The arrangement made possible the detection of atoms submitted to approximately homogenous optical pumping in the radial direction. The effect could be studied as a function of detected beam diameter and several conclusions were drawn relative to the observation of the "peaking" of the signal amplitude versus light intensity. The "peaking" effect predicted in Figs. 5 and 7, could be observed in very specific conditions and a typical result is reproduced in Fig. 10 [26]. In that figure the laser intensity is given in terms of laser driving current and the signal size is given in μA. Consequently, the data cannot be compared directly to the theoretical graphs shown in Fig. 5. Nevertheless, a "peaking" of the signal is observed and the general trend of the signal behavior is observed.

Results obtained by Lewis and Feldman for line width as a function of laser radiation intensity are reproduced in Fig. 11 [39]. An important broadening is observed. Assuming in first approximation that the broadening is linear with light intensity as would be obtained in the homogeneous model [(43) and (38)] and using information contained in [39], one can relate power density used in the arrangement and pumping rate. At a laser radiation density of $250\,\mu\mathrm{W/cm^2}$, calculation gives $\Gamma_\mathrm{p} = 1800\,\mathrm{s^{-1}}$. This situates Lewis graph in the upper portion of Fig. 6 where the line width is nearly linear with pumping rate, making the linear assumption plausible in the present circumstances.

Results obtained by Camparo and Frueholtz relative to contrast at relatively low temperature (37 °C) are reproduced in Fig. 12 [40]. Results for line width are also reproduced in Fig. 13. At that temperature the Rb density is rather low and, as pointed out by the authors, the cell is nearly optically thin. The absorption coefficient measured at that temperature is reported by the authors as $(\tau_D)^{-1} = 7.6\,\mathrm{cm}$. This coefficient is related to $\alpha((\tau_D)^{-1} = \Gamma^*/\alpha)$. At the buffer gas pressure used (10 Torr, N_2), Γ^* is $\sim 2 \times 10^9\,\mathrm{s^{-1}}$, and we obtain $\alpha = 2.63 \times 10^{10}\,\mathrm{m^{-1}s^{-1}}$. The value calculated by means of Rb density (22) from the values used previously is $1.8 \times 10^{10}\,\mathrm{m^{-1}s^{-1}}$. This difference may be due to the difference in density in the cell for a similar temperature, which as pointed out by several authors, may vary considerably depending on the type of glass used and the temperature cycling to which the cell has been exposed prior to measurements [12, 41].

The results presented by the authors on contrast are normalized, and a comparison to previous calculation can be made only on a qualitative basis. Nevertheless, it is readily observed that the general behavior of the saturation ob-

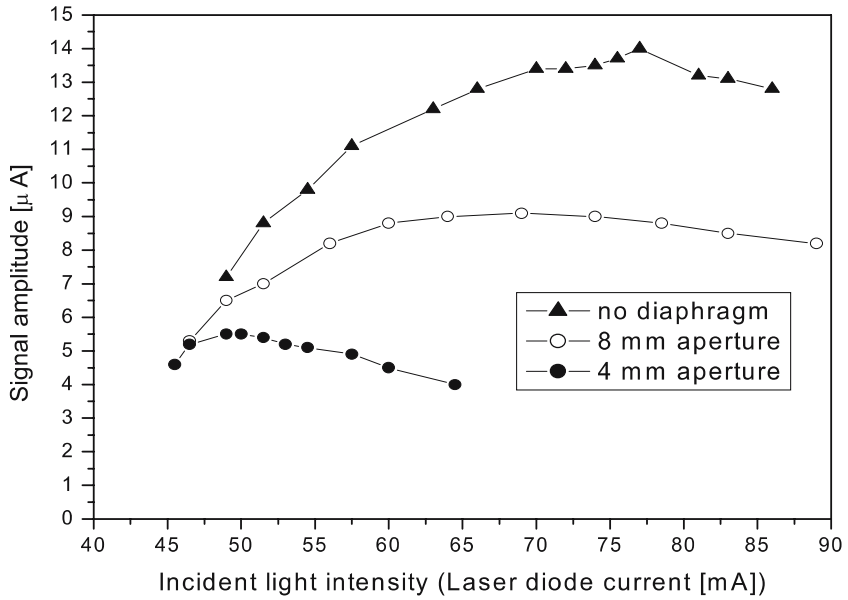

FIGURE 10 Typical result obtained by Mileti for the double resonance signal amplitude as a function of laser radiation intensity in a special experimental arrangement where the laser beam is made homogeneous in radial directions by expansion and portions of the detected transmission signal are selected by means of masks (reproduced from [26] with permission)

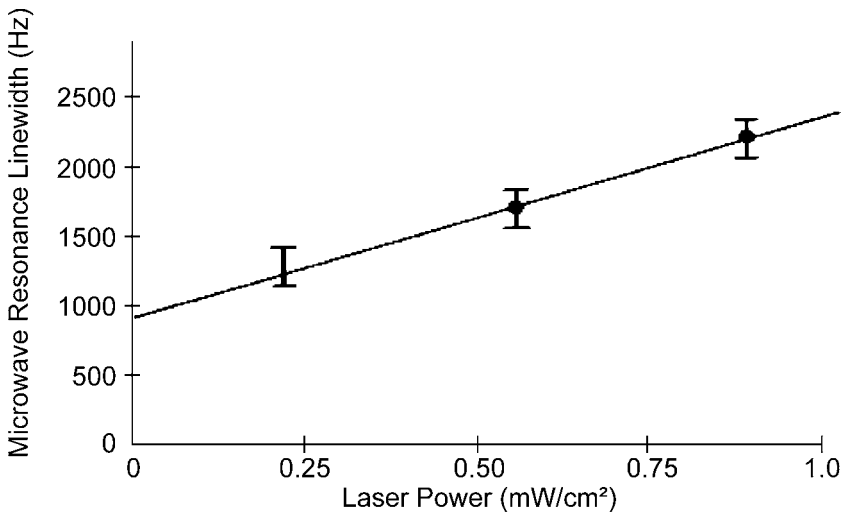

FIGURE 11 Hyperfine resonance line width reported by Lewis and Feldman as a function of laser light intensity (reproduced from [39] © IEEE)

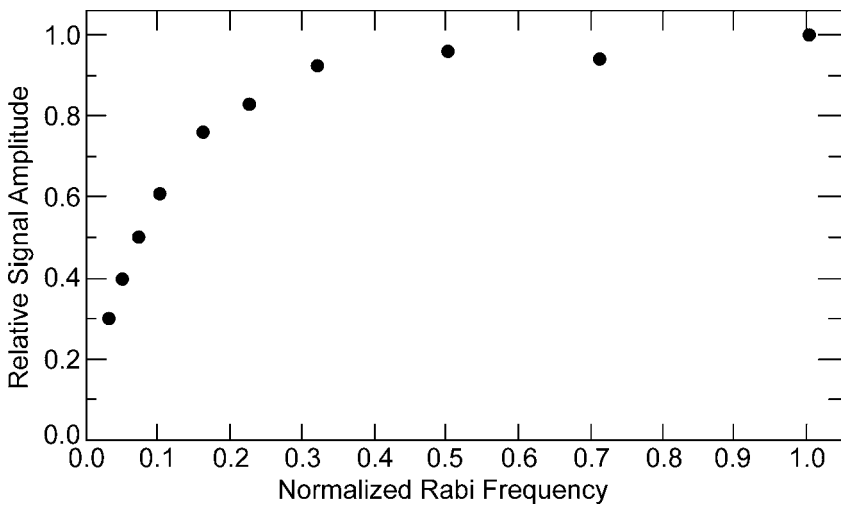

FIGURE 12 Normalized values of contrast versus normalized microwave Rabi frequency observed for the O–O hyperfine transition with laser optical pumping in a Rb cell at 37 °C (reproduced from [40] with permission © 1985 APS)

served in Fig. 12 is the same as that calculated and shown in Fig. 7. The same remark can be made for the data on line width. The large broadening observed in measurements of [40] situates the data in the upper end of Fig. 8 making the broadening linear with the microwave Rabi frequency as expected.

In some cases the signal to noise ratio realized in practice is given for an optimum condition [36, 42–44]. In that case,

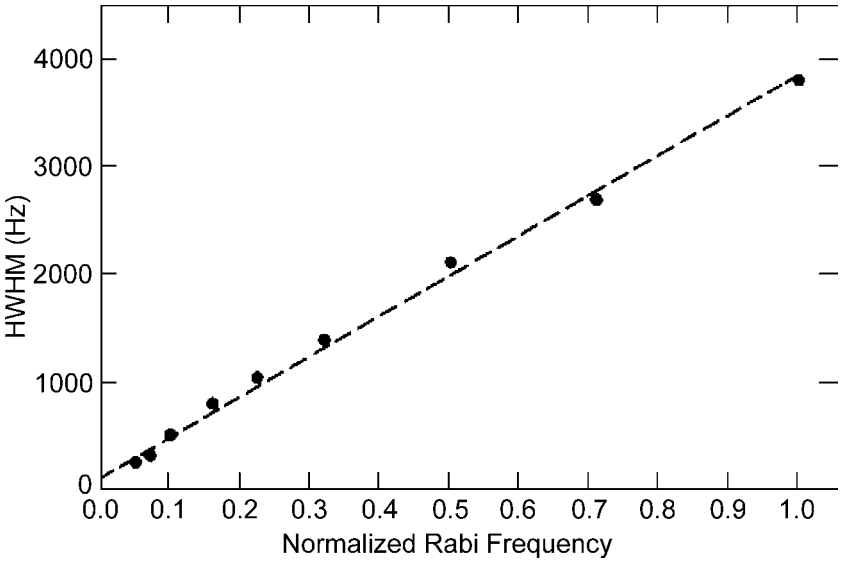

FIGURE 13 Half line width observed as a function of the normalized microwave Rabi frequency for the same situation as that giving the results of Fig. 12 (reproduced from [40] with permission © 1985 APS)

some information on the performance of the system may be extracted. To do so, (1) can be transformed readily in terms of S/N through direct algebraic manipulations [21]. We obtain

$$\sigma(\tau) = \frac{K}{Q_1 \mathrm{S/N}} \tau^{-1/2} , \tag{45}$$

where K is about 0.2, and Q_1 is the resonance line Q, defined as

$$Q_1 = \nu_0 / \Delta\nu_{1/2} \tag{46}$$

Equation (45) provides a simple way of evaluating the performance of the system through a direct measurement of two easily accessible parameters, line width and signal to noise ratio. For example, in [43], using an edge emitting diode, a S/N of 66 dB was reported with a line width of 570 Hz, leading to a predicted frequency stability of $\sim 3 \times 10^{-12}\,\tau^{-1/2}$. In [42], using a DBR laser, with a narrow spectrum ($\sim$ 500 kHz), a S/N of 85 dB was measured and the predicted frequency stability using (45) is $\sim 6 \times 10^{-13}\,\tau^{-1/2}$. In that case, however, the best measured frequency stability was $1 \times 10^{-12}\,\tau^{1/2}$. The difficulty with these reports arises in the absence of information on the actual background radiation level, which would provide a reference to calculate contrast, which, using (1), would then permit an evaluation of the predicted frequency stability and possibly identify the origin of the noise.

The frequency stability predicted on the basis of shot noise alone is not generally realized in practice. A frequency stability of the order of $1\text{–}5 \times 10^{-11}$ is reported when commercial laser diodes having large spectral widths (several tens of MHz) are used as optical pumping sources [39, 45, 46]. Better results are obtained when narrow band laser diodes, such as DBR, DFB, and external cavity locked lasers are used [42, 47–49]. Consequently, noise sources other than shot noise must be present when common diode lasers such as edge emitting lasers and VCSELs are used as optical pumping sources. It is generally recognized that these noise sources originate in part from amplitude fluctuations (AM), inherent to the laser, and laser frequency fluctuations (FM) transformed into intensity noise by the resonance cell [50]. This will be discussed in the section following a description of the various lasers available and their characteristics.

It may be mentioned that approaches have been proposed for increasing the signal to noise ratio by concentrating all the atoms in the $F = 2, m_F = 0$ of the ground state of the Rb atom. This may be done, for example by using a combination of polarized pulses of light and so-called π-RF pulses at the Zeeman frequency [51]. In such an approach, however, the system operates in a pulse mode adding complexity to its practical implementation.

3.7 *Frequency shifts*

Optically pumped sealed cell frequency standards using a buffer gas are characterized by several important frequency shifts. We have introduced above the most important one, the light shift. These shifts affect the accuracy of the standard. Furthermore, their fluctuation with time may affect frequency stability. We will review these shifts in the light of experimental data.

3.7.1 Buffer gas shift. When the atoms are exposed to a traveling microwave field, a buffer gas is required to reduce Doppler broadening through Dicke effect [6]. In the case studied here and represented in Fig. 3, a cavity is used and the atoms are exposed to a microwave standing wave. In such a case, the buffer gas reduces relaxation of the Rb atoms upon collision with the cell inner surface by increasing the diffusion time. In practice, nitrogen is used as one element of the buffer gas in order to quench the fluorescence emitted in the optical pumping process, which would cause random optical pumping equivalent to relaxation [12, 22].

Unfortunately, collisions between the Rb atoms and the buffer gas atoms cause a frequency shift. This shift is proportional to the density of the buffer gas or, in a sealed cell, to its pressure. Furthermore, this shift is temperature sensitive. The Rb hyperfine frequency is shifted by [19]

$$\Delta\upsilon = P\left(\beta_{\mathrm{bg}} + \delta_{\mathrm{bg}} + \gamma_{\mathrm{bg}} \Delta T^2\right) , \tag{47}$$

	β_{bg} [Hz Torr^{-1}]	δ_{bg} [Hz°C^{-1}Torr^{-1}]	γ_{bg} [Hz°C^{-2}Torr^{-1}]
Nitrogen (N_2)	546.9	0.55	−0.0015
Argon (A)	−59.7	−0.32	−0.00035

TABLE 2 Most probable pressure shift and temperature coefficients of ^{87}Rb in buffer gases such as molecular nitrogen and argon

where P is the buffer gas pressure, β_{bg} is the pressure coefficient, δ_{bg} is the linear temperature coefficient and γ_{bg} is the quadratic temperature coefficient. These coefficients have been determined in several laboratories for many buffer gases and most alkali atoms. The pressure and linear temperature coefficients are both positive in the case of N_2. In practice, another buffer gas with a negative temperature coefficient is mixed with nitrogen to minimize the temperature sensitivity of the resonance frequency at a given temperature [52]. The gas most often used is Argon. The characteristics of those two gases are given in Table 2. The numbers have been obtained through an average of the most accurate published data [19].

Equation (47) leads to a quadratic dependence of the frequency as a function of temperature since both δ_{bg} and γ_{bg} cannot be made equal to zero simultaneously. The ratio of the pressure of both gases at cell filling time has to be adjusted such as to position the maximum of the resulting curve at the desired temperature of operation. The behavior just described has been reported experimentally by several authors in both cases of optical pumping with a spectral lamp and with a laser [53–55].

The residual frequency shift of such a mixture is of the order of 200 Hz per Torr. It is not possible in practice to set the total buffer gas pressure to a precision that would provide an accuracy better than $\sim 10^{-9}$. For this reason, even with laser optical pumping, the Rb clock remains a secondary frequency standard and needs to be calibrated.

3.7.2 Magnetic field shift. As in the case of optical pumping with a spectral lamp, a magnetic field is required to provide an axis of quantization to the system and a reference axis for laser radiation. The magnetic field removes also Zeeman degeneracy in the ground state. The $m_F = 0$ sublevels are shifted quadratically causing a shift of the hyperfine frequency according to the equation [19]

$$\Delta\nu_B(^{87}\mathrm{Rb}) = 575.14 \times 10^8\, B_0^2\,\mathrm{Hz}\,, \tag{48}$$

where B_0 is the magnetic induction in Tesla. This field is normally created by means of a solenoid inside a set of concentric magnetic shields. It is of the order of a few tens of μT and produces a shift of the order of 10 Hz. The stability of the current driving this field and the shielding factor of the enclosure must be compatible with the frequency stability desired. Generally, this requirement does not cause major problems.

3.7.3 Light shift. In the three-level model used, only two transitions are considered and the analysis leads to a light shift given by (31) and (32) and plotted in Fig. 9 as a function of laser frequency with the laser intensity as parameter. As discussed above, it should be emphasized that the analysis made was based on several assumptions. The results obtained depend greatly on those assumptions and are to serve mainly as an indication of the size of the effect expected. In this section, we will summarize some of the experimental results reported in the literature and provide some indication on the importance of this shift in the implementation of a practical frequency standard. We will also examine proposals for reducing the effect.

In the analysis of the light shift, it is convenient to introduce two parameters characterizing typical experimental situations. One important parameter is the slope of the dispersion pattern at its center, called the light shift coefficient β_{LS}. It is given by the sum of all light shifts that may be included in (31) and (32). Close to one optical resonance line originating from one of the ground state hyperfine levels, the shift from the other transition is small and the light shift, $\Delta\omega_{LS}$, may be written rather as

$$\Delta\omega_{LS} = \beta_{LS}(\omega_L - \omega_M - \omega_{m\mu'})\,. \tag{49}$$

From (32), it is readily shown that β_{LS} is function of the laser power through the pumping rate Γ_p:

$$\beta_{LS} = \frac{\mathrm{d}(\Delta\omega_{LS})}{\mathrm{d}\omega_L} = \frac{\Gamma_p}{\Gamma^*}\,. \tag{50}$$

On the other hand, for a given laser detuning $\Delta\omega_L$ from zero light shift, the resonant frequency is function of the radiation intensity and it is convenient to define the intensity light shift coefficient α_{LS}. We write this shift as

$$\Delta\omega_{LS} = \alpha_{LS} I\,, \tag{51}$$

where α_{LS} close to center of the optical line may be written as

$$\alpha_{LS} = \frac{\Delta\omega_L}{\Gamma^*}\,. \tag{52}$$

It is readily shown by means of (50) that α_{LS}, as defined, is directly related to β_{LS}. The coefficient α_{LS} is very important in practice, particularly when the laser frequency is locked to the maximum of the absorption line used for optical pumping. Such a locking does not guarantee always total independence of the hyperfine frequency against light intensity mainly due to asymmetry in the optical absorption line.

In practice, it is found that the light shift is not linear with light intensity. This is due to saturation effect and the non-homogeneity of the radiation intensity across the laser beam [35]. It is then more convenient to renormalize α_{LS} to a fractional change in light intensity at a given operating laser intensity, that is, fractional frequency shift per percent of light intensity change [56, 57]. We call it $\alpha_{LS(\%)}$. This parameter is more useful than α_{LS} in evaluating the effect of laser intensity fluctuations on the frequency stability of the implemented frequency standard.

Several authors have reported on light shifts and on values of α_{LS} and β_{LS} in particular setups [37, 39, 42–45, 54, 58–63]. When a laser is used without special arrangements for compensating for the light shift, the coefficient β_{LS} is found to be of the order $1–10 \times 10^{-11}$ per MHz detuning of the laser from resonance depending on the laser power applied on the ensemble of atoms. These results are in general agreement with the

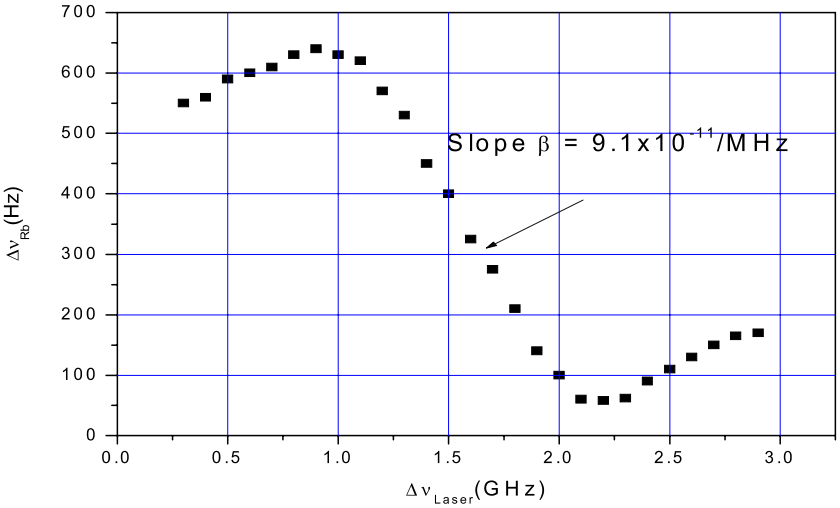

FIGURE 14 Light shift observed in a Rb cell optically pumped with a laser for a laser intensity of 250 μW/cm^2 at 780 nm (D_2) (reproduced from [39] © IEEE)

calculation made above, which gives a light shift coefficient varying from 4.5 to 7.3×10^{-11} for the three Rabi frequencies chosen in the particular example shown in Fig. 9. This agreement is most satisfying in view of the kind of intuitive assumptions and approximation made in the analysis and the absence of information on the buffer gas pressure used in the papers cited. In the past, it was claimed that theory and experiments disagreed by more than an order of magnitude [19]. However, it appears that the conclusion was reached due to an under-valuation of the optical line width.

On the other hand the value of α_{LS} obtained from published data spreads over a wide range. This is due to the size of laser detuning used in its determination. The size of α_{LS} can be evaluated either from (52) or from Fig. 9. For example, for a laser detuned by 250 MHz, that is at the laser tuning for maximum light shift in Fig. 9, we obtain $\alpha_{\mathrm{LS}} = 0.05$ Hz per s^{-1} (in terms of pumping rate). However, in the case that the laser frequency is locked close to the center of the optical absorption line as is normally done, α_{LS} is much smaller by at least an order of magnitude.

A typical example of the phenomenon as measured in a laser pumped ^{87}Rb cell using radiation at 780 nm is shown in Fig. 14 [39]. In this figure, the coefficient β_{LS} is evaluated to be 9.1×10^{-11} per MHz for a power density of 250 μW per cm^2. An evaluation of $\alpha_{\mathrm{LS}\%}$ can also be made from the data reported by the authors [39]. At maximum light shift we obtain $\alpha_{\mathrm{LS}\%}$ as 4.9×10^{-10} per percent change in light intensity. In order to compare these results to those obtained in the previous analysis, the pumping rate must be known. The authors of [39] provide information on the hyperfine resonance line broadening as a function of laser power density. From this information, assuming a saturation factor of the order of 1, providing a contrast of 10% as reported, we evaluate the pumping rate by means of (43) to be 1800 s^{-1} at a power density of 250 μW/cm^2. At that pumping rate, our analysis gives $\beta_{\mathrm{LS}} \cong 4 \times 10^{-11}$ per MHz laser detuning and $\alpha_{\mathrm{LS}\%} \cong 2 \times 10^{-10}$ per percent change in light intensity, values that fall in the range of those obtained in our calculation. These shifts are rather large and may affect the performance of the frequency standard through various mechanisms. When the laser is not tuned to the frequency where the light shift is zero, there can be direct conversion of laser intensity fluctuations into frequency instability of the clock.

Quasi-static laser frequency fluctuations that affect clock frequency stability in the long term are minimized by locking the frequency of the laser to the center of the optical absorption line in the resonance cell. This is the simplest approach. However, the optical absorption line is broadened by the buffer gas (> 750 MHz) and the frequency lock is generally weak. Furthermore, this optical line is a combination of several absorption lines corresponding to transitions from the ground state to the various hyperfine levels of the P state. In such a case, the light shift may not be zero and there may be a residual dependence of the frequency on the laser intensity. Another approach consists of locking the laser frequency to an external cell without buffer gas by means of saturated absorption of a chosen hyperfine line. The saturated absorption line width is of the order of 5 MHz [54, 64–66]. In that technique, an extra cell is required raising the complexity of the system. Furthermore, the laser frequency is not locked to the same frequency as that of the maximum absorption in the resonance cell. In such a case, there remains a shift dependent on light intensity, unless the laser beam frequency is translated by such means as an acousto-optic modulator.

Several proposals have been made for reducing the light shift. In one approach, it was proposed using a high buffer gas pressure in the resonance cell in order to broaden the optical resonance absorption line [56, 57, 67]. The added broadening reduces the slope of the dispersion curve at the center of resonance and makes the clock frequency less sensitive to laser frequency and intensity fluctuations. There is a net advantage in using this approach, but at the expense of a weaker lock of the laser frequency to the absorption line. With a pressure of 100 Torr, the laser tuning sensitivity (β_{LS}) was reduced to $\sim 6 \times 10^{-13}$ per MHz laser detuning [57]. The sensitivity to laser intensity ($\alpha_{\mathrm{LS}\%}$) was measured as $\sim 10^{-11}$ per 1% change in light intensity for the laser locked to the broadened optical resonance line.

Another approach consists of introducing in the laser spectrum, sidebands that compensate the light shift of the main carrier [68, 69]. This is similar to the technique used in the implementation of frequency standards using the coherent population trapping phenomenon [70] in order to avoid light

shifts by selecting a proper index of modulation of the laser. The authors claim a complete cancellation of the light shift by a proper choice of the modulation index. Another similar approach uses two lasers [71]. This last technique has the added advantage of populating the $F = 2$, $m_F = 0$ level at the expense of the other Zeeman levels of the ground state.

An interesting technique has been proposed by Hashimoto and Ohtsu [44] for tuning automatically the laser frequency to obtain zero light shift. It is based on the observation that when the laser frequency is detuned from exact optical resonance, the observed hyperfine resonance line becomes asymmetrical under special circumstances such as inhomogeneous broadening caused by a variation of laser intensity in the radial direction [35]. That property leads to the possible implementation of a system that measures the asymmetry, interpret it in terms of frequency, and control the laser frequency such as to reduce the asymmetry to a minimum. In principle, the technique leads to zero light shift. The authors claim that using that approach, the long term frequency stability of the clock they implemented was improved by a factor of 45 as compared to the case where the laser was not locked using that technique [44]. They report that the resulting observed frequency drift was reduced to 6.3×10^{-13} per hour. However, it may be mentioned that this drift corresponds to 7.6×10^{-11} per month and is larger than that observed in similar standards using a spectral lamp.

In a technique proposed by Camparo and Delcamp [72, 73], a natural Rb cell is used and ground state population inversion of the ^{87}Rb isotope is done by means of the fluorescence of ^{85}Rb optically pumped by a laser. The coincidence of optical lines allows optical pumping with specific properties regarding light shift. The authors claim that the frequency dependent light shift (β_{LS}) is reduced by at least an order of magnitude. However, the intensity dependent light shift (α_{LS}) is increased by an order of magnitude.

Other methods consist of pulsing the laser radiation and observing the hyperfine resonance signal in the dark [74, 75]. In principle, since there is no light present during the observation of the resonance signal, the light shift should disappear totally. Such an approach has been implemented in combination with the use of the Ramsey separated pulse technique in time rather than space [64]. The light shift was reduced to 3×10^{-13} /MHz. Another similar approach, proposed in the 1960s [76] with a spectral lamp makes use of stimulated emission in a cavity. In that case, the optical radiation is pulsed and two Ramsey microwave pulses are applied in succession. Stimulated emission is observed after these microwave pulses, Ramsey fringes being observed after the second pulse. In such a case a high Q cavity is required for the observation of stimulated emission and the system is essentially an Rb maser below threshold. This approach was implemented recently by Godone et al. using intense laser radiation to destroy any ensemble residual microwave coherence between the optical pumping cycles [77, 78]. The results will be reviewed in a later section of this paper.

Although these pulsing techniques appear to be rather effective, they add complexity to the system. There is also the possibility of the presence of a so-called "position shift" created by inhomogeneities in the ensemble [79]. Such an inhomogeneity could be created for example by a magnetic field gradient. In such a case, the average resonance frequency of the ensemble may depend on the light intensity, after the light has been turned off, since different regions of the resonance cell may be weighed differently, depending on the optical thickness of the ensemble.

The analysis of the effect of rapid fluctuations of the laser frequency and intensity on the clock behavior requires a knowledge of the spectral density of frequency and intensity fluctuations of the laser. This analysis is delayed to Sect. 4.4.

3.7.4 Spin exchange frequency shift. Spin exchange interaction taking place in collisions between alkali atoms causes relaxation of the population and of the coherence that exists in the ground state. The relaxation has been taken care of above in introducing it phenomenologically in the rate equations through γ_1 and γ_2. These rates are given by [19]

$$\gamma_1 = n\langle v_{\mathrm{r}}\rangle\sigma_{\mathrm{se}} \tag{53}$$

$$\gamma_2 = \frac{6I+1}{8I+4} n 2\langle v_{\mathrm{r}}\rangle\sigma_{\mathrm{se}}\,, \tag{54}$$

where n is the alkali atom density, $\langle v_{\mathrm{r}}\rangle$ is the relative velocity of the atoms, σ_{se} is the collision cross section, and I is the nuclear spin. Values of σ_{se} as measured by various authors have been tabulated in [19]. For a temperature of 60 °C the density of Rb is $\sim 3 \times 10^{11}\,\mathrm{cm}^{-3}$ and $\langle v_{\mathrm{r}}\rangle$ is 400 m/s. In the case of ^{87}Rb, $\sigma = 1.8 \times 10^{-14}\,\mathrm{cm}^2$, the rate γ_1 is $216\,\mathrm{s}^{-1}$ and γ_2 is $135\,\mathrm{s}^{-1}$. The spin exchange contribution to the line width is thus 43 Hz. On the other hand, such collisions introduce also a phase shift in the magnetic moment of the atom and cause a frequency shift given by the relation

$$\Delta\omega_{\mathrm{se}} = \frac{1}{4} n\langle v_{\mathrm{r}}\rangle\lambda\Delta\,, \tag{55}$$

where Δ is the fractional population difference between the two ground levels, λ is the cross section for such a frequency shift and is calculated as $6.9 \times 10^{-15}\,\mathrm{cm}^2$ [81]. The frequency shift introduced thus depends on the population inversion. In the case of pumping from the lower level, $F = 1$, and total population inversion, the shift is of the order of -8×10^{-12} per K. In the situation where the lower level is populated the shift is 1.3×10^{-11} per K. This shift is not negligible and it could very well cause a long term degradation of frequency stability since it is directly proportional to density. It is well known that the establishment of thermal equilibrium in a sealed cell is a very long process [41]. Consequently, it is possible that the phenomenon is in part responsible for long term fluctuations and drift observed in Rb frequency standard in general.

3.7.5 Microwave power shift. If the atomic ensemble is perfectly homogeneous regarding resonance frequency, simple logic leads to the conclusion that the observed resonance frequency should be independent of the microwave power used to observe the resonance signal. The observed frequency should also logically be independent of the shape of the field

mode within the cavity. This is due to the fact that all parts of the ensemble have the same resonance frequency and interrogation of any part with a different microwave intensity does not alter the observed average frequency. However, as was made explicit above, a residual light shift may be present in the ensemble under certain conditions of operation. This light shift varies continuously along the path of the light beam due to absorption as well as transversely since the light intensity may vary in the radial direction. Since the atoms are fixed in space due to the presence of the buffer gas, this causes inhomogeneous broadening of the resonance line. The measured resonance frequency becomes a function of the applied microwave power since different parts of the ensemble have different resonance frequency and are weighed differently due to the shape of the cavity mode and due to saturation effects. It should be realized that any source of inhomogeneity, such as a magnetic field gradient, would create the same effect [82]. This effect is called the power shift. The centre frequency of the resonance line appears to be a function of the power applied. In some practical devices the power shift may be of the order of parts in 10^{10} per dB of RF power fluctuation [19].

This effect was studied using a spectral lamp as optical pumping source [79]. It was shown that the power shift was indeed due to gradients within the cell and the effect was called the "position shift". Risley et al. [82] in more elaborate studies have shown that in a wall coated cell without buffer gas, the atoms being free to move around the cell and to average possible resonance frequency gradients, the power shift disappears completely.

This effect is still present in the case of pumping with a laser and can in fact be amplified since the laser beam intensity varies strongly in the transverse direction. A three dimensional model of the clock incorporating this effect was also made by Camparo and Frueholz [83].

In a setup using a Cs cell with a mixture of Ar-N_2 at 39 Torr, a power shift of 3.8×10^{-10} per dB variation of microwave power in normal operating conditions was observed [61]. A similar result was obtained in the case of Rb [57]. In that case, the cell contained pure isotopic ^{87}Rb in a nitrogen buffer gas at a pressure of 100 Torr. The intent in using such a high buffer gas pressure was to reduce light shift as explained above. The atomic ensemble was pumped with a junction transverse strip laser (JTS) tuned to the D_1 wavelength. The laser was locked to the absorption line either from levels $F = 1$ or $F = 2$ of the ground state and a residual light shift of 10^{-11} /% light intensity was observed. A microwave power sensitivity of 5×10^{-10} /dB was measured. Mileti [26] in preliminary measurements found a microwave power shift of 10^{-11} /dB when the laser was locked to the optical absorption (D_1 transition). A residual light shift of the order of 2×10^{-11} /% light intensity was present.

These results appear to lead to the conclusion that, since a residual light shift exists even when the laser is locked to the center of the optical absorption line, the resonance frequency of the atoms are dependent on their position within the cell. The microwave field varying also with position causes then a dependence of frequency on microwave power, various parts of the cell showing then varying weights on averaging due to saturation of the signal. This conclusion is in agreement with the results found by Risley et al. in the case of spectral lamps [82].

Situations may be found in which the power shift caused by the residual inhomogeneous light shift may be cancelled by a similar opposing effect caused by an intentionally applied magnetic field gradient. This effect was studied in some detail in a spectral lamp pumped standard and it was found that a microwave power independent setting could be found for a given value of the magnetic field which causes cancellation of the inhomogeneous frequency shifts [84].

It may be mentioned that a residual power shift of 10^{-11} /dB as mentioned above requires the microwave generator to be stabilized to 10^{-2} dB to obtain a frequency stability of 10^{-13} in the long term. This may be a difficult requirement to achieve. In such a case, a microwave power stabilizing technique such as that proposed by Camparo based on Rabi resonances could be used [85, 86].

3.7.6 Cavity pulling. The implementation of an Rb frequency standard with laser optical pumping does not alter the effect of cavity tuning on its frequency when compared to optical pumping with a spectral lamp. We recall that in both types of frequency standards the population difference between the ground state hyperfine levels $F = 2, m_F = 0$, $F = 1, m_F = 0$ is the parameter monitored. In that case the clock frequency pulling is given by [19]

$$\Delta\omega_{\text{clock}} = \frac{Q_{\text{cav}}}{Q_{\text{at}}} \frac{\alpha}{1+S} \Delta\omega_{\text{cav}} \tag{56}$$

where Q_{cav} is the quality factor of the cavity, Q_{at} is the atomic resonance quality factor, S is the saturation factor of the resonance, and α may be thought of as a measure of power emitted by the atoms relative to the power absorbed by the cavity. In a typical case, $\alpha \sim 10^{-2}$, $S \sim 2$, $(Q_{\text{cav}}/Q_{\text{at}}) \sim 2 \times 10^{-5}$, and the pulling factor is $\sim 7 \times 10^{-8}$. This is not negligible, as is often assumed in the case of passive standards, and special care must be taken in the design of the cavity and its temperature control in order to have a cavity frequency stability compatible with the long term frequency stability desired. For a required long term frequency stability of $\sim \pm 10^{-13}$, the cavity must stay tuned within ± 10 kHz. Typically a TE_{111} cavity made of copper may have a temperature coefficient of the order of 200 kHz per degree [87]. This means that a temperature stability of ± 50 millidegrees over long periods is required to achieve a frequency stability of $\pm 10^{-13}$.

It should also be mentioned that according to (56), a change in cavity Q with time may have an important effect on long term stability even if the cavity is perfectly tuned. This is due to the fact that a change in cavity Q will affect the microwave intensity at the resonance cell, which in turn could affect the residual power shift. This was studied in some detail by Coffer et al. who found that cycling of cavity temperature was affecting Rb distribution within the cell causing metallic deposits on the cell walls and causing degradation of cavity Q [88]. This is an effect that can affect the long term frequency stability of the frequency standard.

4 Laser characteristics

During the last two decades, solid state laser diodes required for the implementation of optically pumped frequency standards have known an intensive development. In this section we will give an overview of the characteristics of those readily available diode lasers, discuss their qualities when integrated in a frequency stabilizing systems, and finally analyze their influence on the frequency stability of frequency standards when they are used as optical pumping sources.

4.1 *Types of lasers available*

A wide variety of diode laser designs have been used in optical pumping. For our purpose, these can be divided into two general classes, edge-emitting lasers that emit coherent light parallel to the boundaries between the semiconductor layers, and surface-emitting lasers (VCSEL) that emit coherent light perpendicular to the boundaries between the layers. Since the power density required in the present application is less than a few hundreds of microwatts per cm^2, we will limit the discussion to low power lasers, that is those diode lasers that emit a total power of the order of a few mw. The edge emitting diode has typically a spectral emission line width of the order of 20 to 50 MHz while the spectral width of VCSEL is of the order of 50 to 100 MHz.

Unfortunately, edge emitting laser diodes have the undesirable characteristics of mode hopping when either temperature or driving current are altered to adjust wavelength and power. This characteristic makes them, in some instances, unusable since the wavelength desired cannot be realized in practice. Diodes with the appropriate wavelength are then selected. In general the yield is very low, 80% of the diodes with wavelength outside the range desired. On the other hand, VCSELs have been designed in general with an internal configuration that prevents mode hoping and, thus, are better adapted to the application reviewed.

The VCSEL has several other advantages over edge-emitting diodes. The VCSEL is cheaper to manufacture in quantity, is easier to test, and is more efficient requiring less electrical current to produce a given coherent energy output. The VCSEL emits a narrow, more nearly circular beam than traditional edge emitters; this makes easier the manipulation of the laser beam such as coupling into an optical fiber.

Other types of lasers, showing interesting characteristics regarding spectral line width are available. These are special constructions edge emitting laser diodes such as distributed Bragg reflector type lasers (DBR), or distributed feedback construction (DFB). They have narrow emission spectra ($<$ a few MHz).

4.2 *Spectral width, phase noise, intensity noise*

As made explicit in (1), the short-term frequency stability of laser-pumped frequency standards is determined by noise from a number of sources. When lasers are used, intensity noise and phase noise may affect the clock frequency stability through various mechanisms. Direct detection of intensity fluctuations at the photodetector, FM-AM conversion noise in the resonant cell, as well as FM conversion through the light shift may affect the frequency stability of the implemented frequency standard. Therefore, a characterization of phase noise and intensity noise, of the lasers used is of prime interest. We will limit the study to those laser diodes that have been used and show promises in the implementation of the IOP double resonance frequency standard presently under study.

4.2.1 Laser phase noise. Phase fluctuations in laser originates from many sources such as spontaneous emission and mechanical instabilities of the structure. The first source is important in diode lasers and generally leads to white frequency noise. We call $S_\phi(f)$ [rad^2/Hz] and $S_\nu(f)$ [Hz^2/Hz] the phase and frequency spectral density of phase and of frequency fluctuations, respectively. They are related through the relation

$$S_\nu(f) = f^2 S_\phi(f)\,, \tag{57}$$

where f is a Fourier frequency. The laser emission spectrum is generally Lorentzian and its width originates primarily from these phase or frequency fluctuations. An approximate value of the noise spectral density in the case of white frequency noise may be obtained from the laser emission spectrum through the relation [89]

$$\Delta\nu_{1/2} \cong 2\pi S_\nu(f)\,. \tag{58}$$

This relation should be used with caution since it assumes that he laser frequency fluctuations are constant with frequency (white). For DBR and DFB lasers the line width may be of the order of a few MHz or less and for VCSELs it may be 50 to 100 MHz. Consequently the phase spectral density varies widely depending on the type of laser used. As will be shown below, it is possible to reduce the spectral width of lasers to a few hundred kHz by means of special extended structures in which the laser is part of a resonator acting as a high Q cavity. In that case, the laser frequency fluctuation spectral density is considerably reduced.

As an example, the phase spectral density of a DFB laser is shown in Fig. 15 [90]. The frequency noise spectrum is nearly white with $S_\nu(f) \sim 10^6$ [Hz^2/Hz], which according to (58) gives a spectral width of ~ 6.3 MHz. The measured width was of the order of 7 MHz. Mileti has reported a spectral density for a free running laser and for the same laser locked to an absorption line. In the case of the locked laser, the noise appeared to be nearly white, was reduced by a factor of about 50 at a Fourier frequency of 300 Hz, when compared to the free running situation, and its measured frequency fluctuations spectral density was 16×10^6 [Hz^2/Hz] [26].

4.2.2 Relative intensity noise. The noise spectral density of the photocurrent fluctuations at the output of a detector illuminated by an optical source may be written as

$$\mathrm{PSD}_{\Delta I}(f) = 2eI_{\mathrm{ph}} + I_{\mathrm{ph}}^2 \mathrm{RIN}(f)\,, \tag{59}$$

where I_{ph} is the average value of the output photocurrent, e is the electron charge. The first term on the right-hand side of (57) is the shot noise introduced in (4). The second term represents the power spectral density of the relative intensity

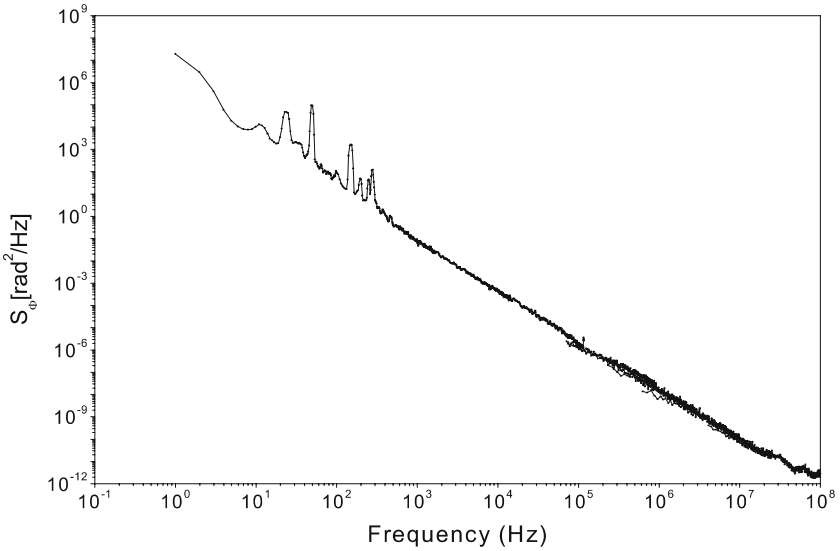

FIGURE 15 Spectral density of phase fluctuations of a DFB laser [90]

fluctuations. These are characterized by the relative intensity noise parameter of the source (RIN) defined as

$$\mathrm{RIN} = \frac{(\mathrm{PSD})_{\mathrm{in}}}{I_{\mathrm{ph}}^2} \tag{60}$$

and the RIN is generally a function of frequency. Laser diodes intensity noise has been the subject of numerous studies and reports have been written on its characterization for several types of lasers [26, 90–93]. In general RIN is a complex function of frequency and laser driving current. A typical result of measurements made at 1 kHz is shown in Fig. 16 for various lasers, Fabry–Pérot (FP) and distributed Bragg reflector (DBR) types [92].

Mileti [26], reports a RIN of 2.8×10^{-13} /Hz for an edge emitting diode laser at a frequency of 300 Hz and a current about 70% above threshold. This is of the order of magnitude of the results shown in Fig. 16 for the Fabry–Pérot lasers. Results on a DBR laser show a RIN of the order of 10^{-13} /Hz at a driving current 50% above threshold. Saburi et al. reports also a RIN of the order of 10^{-13} /Hz for a DBR laser having a spectral line width of 500 kHz [42]. On the other hand, the RIN of VCSEL diodes is a complex function of frequency and driving current and is generally larger than the RIN of edge emitting diodes.

It may be added that solid state laser diodes may be characterized by the presence of a residual broadband spectrum spreading over several nanometers [26]. To the authors knowledge, no work has been reported on its effect on the frequency stability of a laser pumped frequency standard. In principle it would add directly to the intensity noise at the detector, since that radiation is not absorbed by the cell.

4.3 *Laser line width reduction, laser frequency and intensity stabilizing techniques*

The frequency and power output of free-running laser diodes is very sensitive to small changes in injection current and temperature. Consequently, in view of the analysis made above in connection to the effect of laser frequency and intensity on light shifts and pumping rates, it appears of importance that both the intensity of the laser and its frequency be stabilized. Unfortunately, these two requirements may be incompatible in practice since the adjustable parameters that

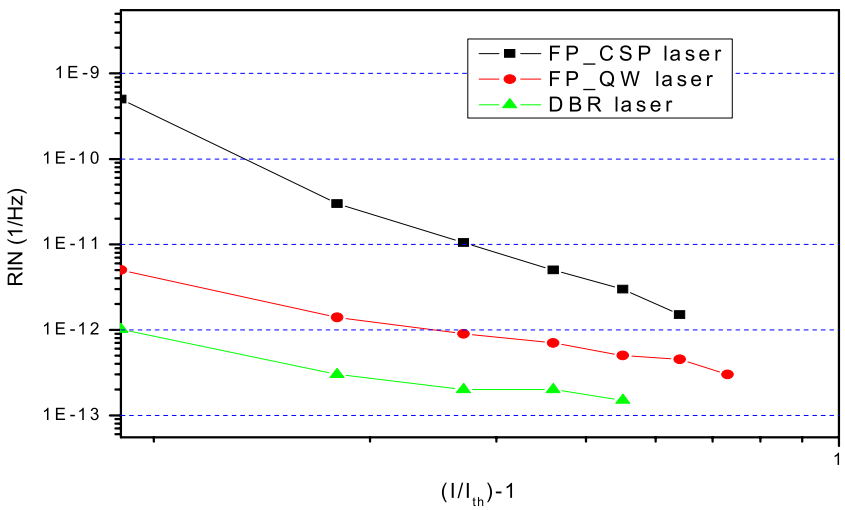

FIGURE 16 Relative intensity noise as a function of laser driving current at the frequency 1 kHz [92]. FP stands for Fabry–Pérot construction and QW stands for quantum well. The FP_CSP laser is a single mode GaAlAs laser. DBR stands for distributed Bragg reflector

are available to perform each task in the most direct and simple approach, that is laser driving current and temperature, are not independent [94]. Furthermore, as will be seen below, the spectral width of the laser may have a direct effect on short term frequency stability of the Rb frequency standard. It is, thus, important to examine possibilities of reducing the laser line width.

4.3.1 Line width reduction. Several techniques, either optical or electronic, have been devised to narrow the emission line width of diode lasers. Excellent reviews of these techniques have been published [95, 96]. We will mention here those most important for the present application.

Simple optical feedback. It is possible to force a multimode laser diode to oscillate on a single mode by providing optical feedback from a small mirror or glass plate placed close to one of the laser facets. The limitations to this method are that it does not work with all lasers, and still requires some sort of frequency reference to stabilize the laser frequency. Furthermore, it can be difficult to achieve long-term stable performance with such systems [97–99].

External cavity lasers. In that approach, the system uses feedback from a frequency selective elements such as a grating to provide a narrowband continuously tunable source of light. A variety of geometries are possible. The diffraction grating is mounted in either a Littrow or in a Littman configuration, in which the light diffracted into the first order returns to the laser. The main difference between these two configurations resides in the technique used to reflect radiation back to the laser from a selected order diffracted by the grating. These are generally called extended cavity diode lasers (ECDL). The spectral line width for such configurations is strongly dependent on the feedback and also on the ratio between external cavity and diode cavity lengths. Line widths of the order of one hundred kHz are achievable. Over long periods, various noise sources (acoustic wave propagation, air movements, driving current instabilities, mechanical and thermal drifts) contribute to broaden the line width. The line width can also be temporally affected by phase fluctuations of the reflected light induced by the mechanical vibration of the external reflector [100].

Feedback from high-Q optical cavities. The essence of the optical feedback methods is that by increasing the quality factor (Q) of the laser's resonator, the line width is reduced. The simplest implementation of the optical method for spectral narrowing is just to reflect back to the laser a small fraction of its output power. Using this technique, one can reduce the line width by more than a factor 1000 achieving line width of a few kilohertz [101–103].

Electrical feedback. Spectral line width reduction can also be accomplished by means of electrical feedback derived from the laser spectrum as measured with a Fabry–Pérot interferometer [104]. In that implementation, the minimum value obtained was 330 kHz for an InGaAsP laser at 1.5 μm, which was 15 times narrower than that of a free-running laser.

Other approaches. Kozuma et al. [105] proposed an optical feedback method to control a semiconductor laser frequency by utilizing velocity-selective optical pumping (VSOP) and polarization spectroscopy of a rubidium (^{87}Rb) atomic vapor. In this way the laser field spectral line width was reduced to 20 times less than that of a free running laser. Another approach to reduce the laser emission line width consists of placing the laser diode inside a relatively long cavity, with some means of wavelength selection [106, 107]. This technique narrows the laser line width and provides a means of tuning the laser to any desired wavelength. The disadvantage is that it requires high quality antireflection coatings on the laser diode and a stable mechanical structure for the external cavity.

4.3.2 Laser frequency stabilization. In the analysis made above, it was concluded that in a typical situation the light shift coefficient β_{LS} could be as large as 5×10^{-11} per MHz laser detuning. This sets the requirement that the laser frequency be stabilized to ~ 2 kHz to achieve a clock frequency stability of 10^{-13} over long term periods. This is not a trivial requirement.

In practice, the long term stabilization may be done by means of a frequency locking to an atomic resonance line. The most common and simplest approach consists of locking the laser frequency to the linear optical absorption line observed in the same resonance cell as that used in the frequency standard, as shown in Fig. 3. However, this absorption line is rather large (700 to 1000 MHz), being broadened by the buffer gas. Consequently, this approach requires a tight frequency lock to a few parts in 10^6 of the absorption line width. It is also possible to lock the laser to a saturated absorption line in an external cell. In that case the width of the absorption line is of the order of 5 MHz and the task of the frequency control loop is relaxed to stabilizing the laser frequency to a few parts in 10^4 of the absorption line width. In both cases the locking of the laser frequency is generally done by low frequency modulation of the laser frequency through the driving current and synchronous detection, the error signal developed being applied to the current driving source as shown in Fig. 3.

In general, laser frequency stability is evaluated over short term periods below 1000 s. This is a range where measurements can be made easily and information on the characteristics of the frequency lock loop efficiency can be obtained rapidly. For example, Tsushida et al. [108] evaluate from the error signal developed in the servo loop a laser frequency stability of the order of $10^{-11}\ \tau^{-1/2}$ for $10^{-2}\ \text{s} < \tau < 100\ \text{s}$, using stabilization on the D_2 linear absorption line of ^{85}Rb in a cell without buffer gas. In such a case the optical absorption line width is Doppler broadened and is of the order of 500 MHz, which may limit the efficiency of the locking system. At averaging times longer than 100 s, laser frequency stability appeared to degrade rapidly. Similar results were reported by Ohtsu et al. [104], and Hashimoto and Ohtsu [43], using the D_2 absorption line of ^{87}Rb as the reference. It should be mentioned that in those cases laser frequency stability was inferred from the error signal in the servo loop and results regarding frequency stability may have been optimistic. In experiments of the same nature in which a laser was frequency stabilized to linear absorption in a Rb cell, the beat frequency between

two such lasers was measured and frequency stability was evaluated to be $4.2 \times 10^{-10}\,\tau^{1/2}$ for the range 0.2 to 40 s and $\sim 10^{-11}\,\tau$ for longer periods, probably caused by drift [109]. In later experiments, Barwood et al. used saturated absorption technique and a laser whose line width was narrowed by optical feedback. In that case, a frequency stability measured directly from the beat frequency between two such stabilized lasers gave $1.9 \times 10^{-11}\,\tau^{1/2}$ [110]. At 10 s a laser frequency stability of 4×10^{-12} was observed corresponding to fluctuations of the order of 1.5 kHz, degrading slightly above that averaging time. In measurements made over several months, however, the laser frequency could be reproduced only to about 44 kHz.

Beverini used the dichroic property of a Cs vapor in a magnetic field for stabilizing the frequency of an external cavity diode laser system in Littman configuration [111]. Although the width of the absorption line used for locking is still Doppler broadened, the technique, called DAVLL for dichroic-atomic-vapor laser lock, provides a much larger signal than that obtained by means of saturated absorption and is particularly robust against mechanical perturbations. It also offers a series of advantages requiring fewer optical and optoelectronic components and no frequency modulation of the diode laser current.

More recently, Affolderbach and Mileti [112–114] have reported measurements on extended-cavity diode lasers (ECDL), stabilized to Rb reference cells by means of saturated absorption. Their results are reproduced in Fig. 17. It is readily observed that the laser stabilized on Doppler broadened line gives a frequency stability of the order of 10^{-10} in the range of 10 000 s reflecting frequency fluctuations of the order of 375 kHz. Following the discussion made above relative to the possible presence of a light shift of the order of 5×10^{-11} per MHz laser detuning, it is quite evident that such laser frequency fluctuations could be a handicap on long term frequency stability of the clock. It should be mentioned, however, that the results obtained by means of locking to saturated absorption were better than those obtained by Barwood [110], probably due to a tighter lock.

4.4 *Impact of laser instability on clock frequency stability*

In Sect. 4.3.2 we have examined the effect of slow laser frequency fluctuations on the long term frequency stability of the frequency standard. In the present section we wish to address the effect on frequency stability of the clock of rapid fluctuations of the intensity and frequency of the laser, in other words the effect of laser frequency fluctuations at Fourier frequencies that would affect the clock frequency stability in the short term region (< 100 s).

4.4.1 Laser intensity fluctuations. Laser intensity fluctuations have been characterized above by means of the relative intensity noise concept RIN. For an edge emitting laser diode the RIN may be of the order of $5 \times 10^{-13}\ \mathrm{Hz}^{-1}$ at a frequency of 200 Hz and depends slightly on the frequency at which it is determined [26]. This noise, modulating the amplitude of laser radiation, is transmitted through the resonance cell, and is detected by the photodetector as noise directly added to the shot noise component. Using this value and the numbers used before for the hyperfine resonance line characteristics (contrast = 10%, $\Delta\nu_{1/2} = 500$ Hz) (1) predicts a frequency stability better than 10^{-13}. It is, thus, concluded that noise detected directly at the photodetector originating from laser intensity noise cannot be responsible for the measured frequency stability of 10^{-11} using such diodes. However, VCSELs are known to have much larger RIN and may cause observable frequency instabilities in the short term.

Laser intensity fluctuations can also influence the frequency stability of the clock through the light shift. In the case that the laser tuning and locking is such as to leave a residual light shift, laser intensity fluctuations ΔI are converted into clock frequency fluctuations $\Delta\nu_{\mathrm{LS}}$ through the dispersion pattern of the light shift. We call S_{LS} the slope of this light shift against current at the detector:

$$S_{\mathrm{LS}} = \Delta\nu_{\mathrm{LS}}/\Delta I \tag{61}$$

and the frequency instability of the frequency standard caused by this process may be written:

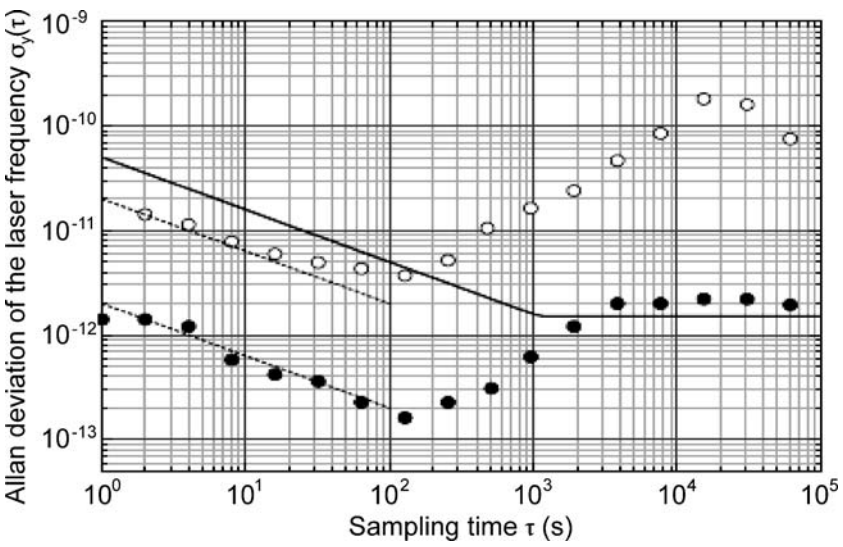

FIGURE 17 Allan standard deviation of lasers stabilized on linear absorption (*open circles*) and saturated absorption (*filled circles*). *Dashed lines* correspond to short-term stabilities of $2 \times 10^{-11}\,\tau^{-1/2}$ and $2 \times 10^{-12}\,\tau^{-1/2}$ for each scheme respectively. The *solid line* illustrates typical stability required to avoid important light shift effects as discussed in the text (reproduced from [113] with permission)

$$\sigma(\tau) = \frac{1}{\sqrt{2}} \frac{(\mathrm{RIN})^{1/2} \times I \times S_{\mathrm{LS}}}{\nu_0} \tau^{-1/2} . \tag{62}$$

With a laser locked to the optical absorption line in the cell, the residual S_{LS} as mentioned above may be of the order of 5×10^{-11} per 1% change in light intensity at the photodetector. In that case with a RIN of $5 \times 10^{-13}\,\mathrm{Hz}^{-1}$ we obtain $\sigma(\tau) = 2.5 \times 10^{-16}$, a totally negligible contribution. Even if the RIN, as may happen in certain VCSELs, is increased by two orders of magnitude the contribution would not be visible at the level of frequency stabilities observed presently.

4.4.2 Laser frequency fluctuations. In the short term, the frequency fluctuations of the laser may affect the clock frequency stability through several processes such as, the frequency lock loop of the laser itself, the light shift, and non-linear optical absorption in the cell.

In the first case, the process consists of a conversion of laser frequency noise through the discriminator pattern of the optical frequency lock-loop. If the servo system has a broad band, rejecting laser fluctuations at frequencies greater than the modulation frequency of the RF generator, the effect, in principle, should be negligible. However, higher frequency noise components may create beat notes between high frequency components and may lead to lower frequencies, which appear as amplitude noise. This adds directly to the shot noise component. The process is rather complex, but a rough evaluation shows that the noise generated may be of the order of magnitude of shot noise [26].

In the second case the laser frequency fluctuations are transformed into clock frequency fluctuations through the dispersion pattern of the light shift. The effect on the frequency fluctuations of the clock in the frequency domain, $S_\nu(f)_{fs}$, can be evaluated through the expression

$$S_\nu(f)_{fs} = S_\nu(f)_{\mathrm{laser}} \times \beta_{\mathrm{LS}}^2 , \tag{63}$$

where $S_\nu(f)_{\mathrm{laser}}$ is the laser frequency fluctuations spectral density and β_{LS} is the light shift coefficient defined through (50). The laser spectral density is a function of the optical servo loop bandwidth and may be of the order of several $\mathrm{kHz/Hz^{1/2}}$. On the other hand, as reported above, β_{LS} may be of the order of $5\text{–}10 \times 10^{-11}$ /MHz. For the purpose of calculation of an order of magnitude, we assume a $S_\nu(f)_{\mathrm{laser}}$ for the DFB laser reported above, $10^6\,\mathrm{Hz^2/Hz}$ and a $\beta_{\mathrm{LS}} = 1 \times 10^{-10}$ /MHz or 0.68 Hz per Hz of laser detuning. Assuming white frequency noise the calculated clock frequency stability is then

$$\sigma(\tau) = 7 \times 10^{-14}\, \tau^{-1/2} , \tag{64}$$

a negligible value. In the case of an edge emitting laser locked to linear absorption in the cell mentioned earlier the $S_\nu(f)_{\mathrm{laser}}$ is $16 \times 10^6\,[\mathrm{Hz^2/Hz}]$ and the effect on frequency stability is $\sim 3 \times 10^{-13}$.

In the third case, the laser frequency fluctuations (FM) are converted into amplitude fluctuations (AM) by nonlinear resonant absorption processes within the resonance cell [115, 116]. When resonant laser light passes through the vapor, the laser intrinsic phase fluctuations induce random variations in the medium absorption cross section [117–120]. This phenomenon has feedback on the transmitted radiation and as a consequence laser phase noise (PM) is converted into transmitted laser intensity noise (AM). This process is nonlinear, so that in an optically thick vapor the conversion of PM to AM can increase an optical beam's relative intensity noise by orders of magnitude. In particular, it was found that the resultant RIN after traversal of a cell increased as the square root of the laser spectral width up to a value of the order of the dephasing rate of atoms in the absorption cell. However, it is also found that when the buffer gas dephasing time is much shorter than the field correlation time, or in other words the absorption line width is much larger than the laser spectral width the PM to AM conversion becomes inefficient. An analysis based on the concepts of cross-section fluctuations was found to be in agreement with this observation [120]. Consequently, in order to reduce the effect of FM to AM conversion on clock's frequency stability, it appears that at low buffer gas pressures a narrow laser spectrum is preferable, while at high pressure a wider laser spectrum could be used.

Along this line of thought, several attempts have been made at reducing the effect of laser FM noise on the frequency stability of the laser optically pumped Rb standard. A first approach consists of using a laser with a narrow spectral width. In that case, with the laser frequency locked to an external cell, preferably using saturated absorption, a clock frequency stability well below the 10^{-11} at 1 s has been obtained. For example, Saburi et al. report a measured frequency stability of $1 \times 10^{-12}\, \tau^{-1/2}$ using a DBR laser having a spectral line width claimed to be 500 kHz [42]. On the other hand, a frequency stability of 3×10^{-13} at an averaging time of 1 s was reported by Mileti et al. using a DBR laser with a spectral width of 3 MHz [121]. In that case, however, special care was taken at reducing noise originating from the interrogating microwave generator in order to avoid intermodulation effects to be discussed below. In those two cases [42, 121] the cell contained a mixture of buffer gases, one constituent being nitrogen, but its pressure was not reported.

In an interesting approach, a clone cell was used to cancel passively the intensity noise generated by the clock resonance cell [63]. The technique relies on the correlation of the intensity noise generated in two identical cells through FM–AM conversion. The clone cell is not excited by microwave and serves only at creating an intensity noise correlated to the noise created in the clock cell. It appears that the system, although somewhat complex, is rather efficient in noise cancellation. Frequency stability of $5 \times 10^{-13}\, \tau^{-1/2}$ was reported for a clock using that technique and an extended cavity laser stabilized by means of saturated absorption in an extra cell.

We have mentioned above the system developed by Affolderbach et al. for stabilizing a laser frequency through an extended cavity and saturated absorption [65]. The laser frequency stability obtained should in principle be an excellent optical pumping source for implementing a frequency standard whose frequency stability would not be affected by laser instability in the range of measurements extending to 10^5 s. In fact, the authors have integrated their ECDL saturated absorption stabilized laser in a frequency standard and obtained a clock short term frequency stability of $3 \times 10^{-12}\, \tau^{-1/2}$. Using the Doppler stabilized laser, the authors found that the

frequency stability was worst by an order of magnitude over most of the range of averaging times above 100 s [113].

In another approach, Camparo et al. [57, 67] used a cell containing ^{87}Rb with a nitrogen buffer gas at a pressure of 100 Torr. The optical absorption line width was 1.6 GHz. Optical pumping was done by means of a junction transverse stripe laser (JTS) having a spectral width of 21 MHz and locked to the D, absorption line of the resonance cell. The results are reproduced in Fig. 18. The clock frequency stability is

$$\sigma(\tau) = 1.8 \times 10^{-12}\,\tau^{-1/2} + 1.1 \times 10^{-13}\,\tau^{1/2} \qquad (65)$$

in the range of measurements reported. Since a single resonance cell generates locking signals for both the laser wavelength and the crystal oscillator, the atomic clock has real potential for miniaturization.

4.5 *Intermodulation effect*

Another phenomenon, which appears to have limited the frequency stability of passive frequency standards, has been the so-called intermodulation effect [122]. This effect is present in all types of passive atomic frequency standards and is not connected to the use of lasers for optical pumping. However, it is sufficiently important to be mentioned here. It consists of the so-called aliasing of high frequency noise present in the interrogating signal at even harmonics of the modulation frequency used in the servo loop, to the fundamental frequency in the interrogating signal. An analysis of the phenomenon was made by Audoin et al. in a quasi-static approach [123]. It was shown that the main effect was due to noise at the second harmonic of the fundamental modulation frequency f_M:

$$\sigma(\tau) = \frac{1}{2}[S_{yLO}(2f_M)]^{1/2}\tau^{-1/2} \qquad (66)$$

A simple calculation shows that such an effect using a low quality quartz oscillator as local oscillator could be disastrous leading to a frequency stability in the 10^{-11} range. Verification of the effect was made in various studies using either spectral lamps or laser optical pumping and several approaches were proposed for minimizing the effect. One approach consisted in introducing notch filters at the second harmonic of the modulation frequency at the output of quartz crystal oscillator used as local oscillator [124]. A more direct approach was to reduce the level of noise in the quartz oscillator and following multiplication chain [125, 126]. It was also found, in particular, that the effect could be reduced by using square wave modulation with wide band detection and demodulation at the synchronous detector [127]. The question was addressed in more details using a dynamical analysis [128, 129].

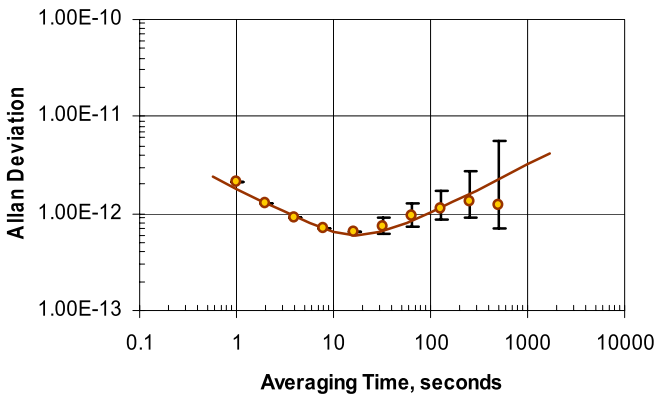

FIGURE 18 Frequency stability of a Rb frequency standard using a JTS (Junction Transverse Stripe) laser as optical pumping source (Camparo, private communication 2007, and [67] © IEEE)

Results obtained in [121] in which the local oscillator characteristics were such as to minimize intermodulation effects are reproduced in Fig. 19. The setup uses a DBR laser for optical pumping source locked to a cross-over transition saturated absorption line in an external cell. It may be added that due to the somewhat pernicious consequences of the intermodulation phenomenon it is not evident that, without particular care, the frequency stability, as reported in several earlier publications for laser pumped passive frequency standards, was not affected by this intermodulation effect. It is obvious that special care needs to be taken in actual implementation of the local oscillator and modulation scheme if ultimate short term frequency stability is the goal aimed for.

4.6 *Long term frequency stability*

The question of long term frequency stability remains a question to be addressed with some attention. In fact there are no a priori reasons to believe that the long term frequency stability of a laser pumped frequency standard will be better than that of a standard using a spectral lamp as pumping source. There were hypothesis advanced in the past regarding the possibility that the light shift could be responsible for the long term drift often observed in standards using a spectral lamp. The question was raised recently by Camparo and the experimental data led to the conclusion that this was an unlikely cause [130]. However, pumping with a laser raises the question to another level. As was discussed above in Sect. 3.3, the light shift may be of the order of several hundred Hz depending on the laser tuning. Consequently, the laser frequency needs to be stabilized with care. In Sect. 4.3.2 results were reported regarding such stabilizing system and it was concluded that, although solutions exist such as using narrow saturated absorption resonance lines, long term laser frequency stability has not been addressed in sufficient details for the particular application considered. Furthermore, in cases where the laser frequency is locked to linear absorption in the clock cell there may remain a light shift that depends on the intensity of the laser radiation. Studies have been made on the possibility of stabilizing both laser frequency and intensity through servo loops on the laser driving current. It was found that the approach led to practical difficulties, the two parameters not being independent [94]. An approach recently used in the control of light shift in a frequency standard based on the coherent population trapping phenomenon may offer a solution to the problem. The technique uses an external LCD intensity control independent of laser driving current. The authors claim excellent results reducing the light shift medium term effect ($100\,\text{s} < \tau < 10\,000\,\text{s}$) by at least an order of magnitude [131].

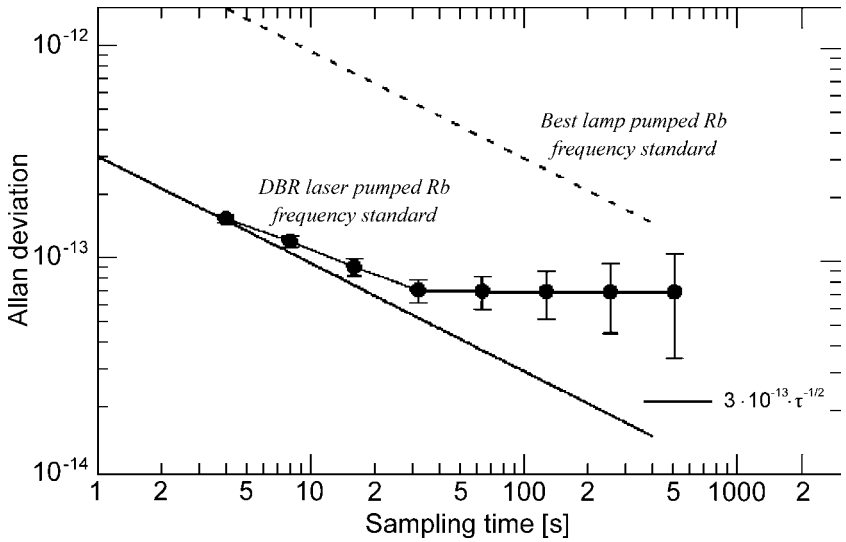

FIGURE 19 Frequency stability reported for passive Rb frequency standard using a DBR laser as pumping source locked to saturated absorption (reproduced from [121] © IEEE). In that case special care was taken to minimize intermodulation effects from the local oscillator. This appears to be the best results obtained for a laser pumped double-resonance Rb system reported to date

The question of long-term drift in sealed cells passive frequency standards thus appears to remain unanswered even using laser optical pumping. The source of the drift observed is still not totally resolved. A possible answer to the question may reside in the recent experimental results obtained by Camparo in the observation of the long time constants required to reach Rb density equilibrium in cells whose thermal equilibrium had been perturbed [41]. It was found that even after hundreds of days, thermal equilibrium was not yet reached under certain circumstances. In that case light absorption varies with time with obvious changes of intensity within the cell and consequences on light shift. Furthermore, changes in Rb density have direct effect on frequency through the spin exchange shift [80]. These combined effects may play an important role in the long term drift as observed in sealed cell Rb frequency standards.

5 Other approaches using a laser with a sealed cell

5.1 *The maser approach*

In the classical approach using a spectral lamp as an optical pumping source, it is possible to create a population inversion such as to obtain self sustained stimulated emission (maser) when such an optically pumped ensemble of ^{87}Rb atoms is placed in a microwave cavity [132]. The main threshold conditions for self sustained oscillation are that the cavity Q be sufficiently large and that a pumping rate compatible with the Rb density be achieved [12]. Such a maser has raised considerable interest due to its excellent short term frequency stability (a few in 10^{13} at 1 s) and its small size. Its properties were studied in detail [133, 134].

It is natural to ask if the cumbersome spectral lamp used in the implementation of that maser could not be replaced by a laser as in the passive approach described above. Attempts were made and self-sustained oscillation could be realized under certain conditions [135–137]. It was found that at the low buffer gas pressure used for maximum gain in the conventional approach, lasers having a narrow spectral width do not provide optical pumping efficient enough to reach oscillation threshold conditions. At low buffer gas pressures, groups of atoms may be off optical resonance due to Doppler shift reducing the number of atoms optically pumped to the upper level. This problem was addressed by modulating the laser frequency in order to cover the cell optical absorption spectrum [135, 136]. At the time of writing, although this IOP Rb maser shows some interesting characteristics, there appears to be little activity on the development of the device at present.

5.2 *The pulsed approach*

In the early 1960s pulsed optical pumping was proposed as an avenue for addressing the light shift problem. The approach used the so-called time domain Ramsey pulse technique [138], microwave stimulated emission in a cavity being the measured parameter [139]. In that early development, the population inversion was accomplished by means of a spectral lamp. That approach was addressed again recently using a laser in order to provide more controllable and more efficient optical pumping [140]. In that case, a strong laser pulse is applied to the ensemble of atoms placed in a microwave cavity resonant at the hyperfine frequency of the atoms. Two short microwave pulses are then applied in succession simulating in the time domain the same conditions on the ensemble as in the classical Ramsey technique applied at two space intervals on an atomic beam. The optical pulse and the two microwave pulses provide a Ramsey stimulated emission cycle. The length and intensity of the microwave pulses are such as to provide a $\pi/2$ atomic excitation and the time between them is less than the decorrelation time due to relaxation processes of the atoms in the cell. Coherent microwave stimulated emission takes place after each microwave pulse. The stimulated emission signal is detected after the second microwave pulse and its amplitude as a function of microwave frequency is characterized by the presence of Ramsey fringes, which can be used, as in the beam approach, to lock the microwave frequency generator to the center of the hyperfine line [141]. The advantage of using a laser is that it allows sufficient power to create a total loss of microwave phase memory between the successive application of the Ramsey cycle. It may be mentioned that the system requires the use of a cavity with a moderate Q (5000 to 10 000). The cell must also be made of low loss material such as quartz to avoid loading of the cav-

ity. Although these requirements appear to introduce some restrictions in design, the results obtained counterbalance this added difficulty in construction. In fact, the results obtained are rather promising relative to the cancellation of the light shift and a short term frequency stability of 1.2×10^{-12} at one second averaging time has been reported [140, 142].

5.3 *Wall coated cells*

According to (1) and (3), a reduction in line width is, in principle, a direct way of increasing frequency stability in the short term. In all practical implementations realized up to now a buffer gas has been used to avoid relaxation caused by collisions of the Rb atoms with the wall of the containing cell. The buffer gas increases the diffusion time to the walls and at pressures above, say 20 Torr, relaxation is caused essentially by spin exchange collisions between the alkali atoms and collisions of the atoms with the buffer gas molecules. The other broadening mechanisms caused by the RF interrogation signal, through the saturation parameter S, and the optical pumping itself, through the pumping rate Γ_p, are also responsible for the resulting line width. Over the years, suggestions have been made on replacing the buffer gas by a non-relaxing wall coating [15, 143]. Much work has been done on the effect of collisions on Zeeman coherences for alkali atoms colliding with surfaces made of long chains hydrocarbon [144]. Such studies have been extended to the case of hyperfine coherence in cells coated with Paraflint© (Moore and Munger) [145]. A relaxation rate of 25 s^{-1} has been measured for ^{85}Rb at the hyperfine frequency of 3.0 GHz in a 6.6 cm diameter cell at 27 C. This corresponds to a line width of 8 Hz. The wall shift was measured and found to be 23 Hz at that temperature. For ^{87}Rb, similar results were obtained, the wall shift being of the order of 130 Hz in a 2.5 cm diameter cell at the same temperature [146]. Although these results, at first sight, appear most promising, it is important to recall that the line width in an operating device is determined also by several other parameters mentioned earlier. For example at an operating temperature of 65 °C, the spin exchange broadening $(5/8n\langle v_r\rangle\sigma)$ is of the order of 65 Hz. In order to optimize signal size and contrast, the optical pumping rate (Γ_p) and microwave Rabi frequency (b) are generally set at a point where line width is doubled in each case. The resulting line width, assuming that wall broadening is negligible compared to those other mechanisms, would be of the order of 260 Hz. Even in the presence of those added broadening, there would still be a net gain in line width in using wall coating compared to buffer gas in which case the operating line width is generally above 500 Hz. It may still be advantageous to operate at lower temperatures where spin exchange is less important. Such an approach needs to be studied experimentally.

On the other hand, temperature dependence of the wall shift may be a handicap for long term frequency stability. In the 2.5 cm cell mentioned above a temperature coefficient of 10^{-10} per °C has been reported requiring a temperature stabilization to ±1 millidegree for a frequency stability of 10^{-13} [146]. Nothing is known either on the long-term stability of the wall shift. It should be mentioned that the light shift, although still present, should have a behavior different from that observed in cells using a buffer gas. Due to the free motion of the atoms this light shift should not produce inhomogeneous broadening and consequently the power shift observed in certain circumstances in cells using a buffer gas should be absent.

The use of laser optical pumping should not alter those conclusions, aside, may be, from an amplification of the effect of internal Ramsey interference line narrowing that has been proposed by Xiao for explaining the somewhat "peaky" aspect of the line shape observed when a narrow laser beam is used for optical pumping [147].

6 Summary and prospects

The classical approach used in implementing a double-resonance passive frequency standard with a spectral lamp as pumping source shows limitations relative to frequency stability mainly due to the resulting large background current that produces shot noise and reduces signal contrast. The frequency stability in typical small units is of the order of $10^{-11}\ \tau^{-1/2}$ for averaging times shorter than 100 s and is normally limited by shot noise. Furthermore, the use of a spectral lamp limits the possibility of a reduction of power consumption as well as size.

The use of a laser diode for optical pumping shows great promises either relative to short term frequency stability, size reduction and at the same time power consumption. The advantages of using a laser diode resides particularly in its narrow spectral width (≤ 50 MHz) relative to a spectral lamp (~ 1 GHz). This provide more efficient optical pumping, reduces the background radiation by orders of magnitude, and consequently reduces shot noise. A calculation shows that a shot noise limited frequency stability better than $10^{-13}\ \tau^{-1/2}$ should be observed in the short term with commonly available edge emitting diodes. However, it is found in practice that using this type of diode a frequency stability less than $10^{-11}\ \tau^{-1/2}$ is observed. It has been shown that this characteristics may have several origins. In particular, the conversion of laser frequency noise to intensity noise (FM–AM conversion) by the cell has been claimed to be a main contributor to the measured limited frequency stability. The laser intensity noise (RIN) appears to play a role only at a level of frequency stability in the range of 10^{-13}.

In some special laboratory configurations, laser-pumped frequency standards have been implemented with frequency stability reaching the 10^{-13} level, close to the shot noise limit, at an averaging time of 1 s. However, these were constructed with elaborate techniques such as extended cavity laser stabilized by saturated absorption in an additional cell, passive noise cancellation by means of an extra clone cell, or still using rather costly DBR or DFB lasers.

In the long term, that is for stability over hours or days it appears that the light shift may be an important factor in the determination of frequency stability if the laser is not well stabilized and tightly locked to the optical resonance line used to create the optical pumping. Even in that case the locking frequency may not be corresponding to zero light shift and a residual intensity dependent light shift may be present.

It appears at present that if the conditions, small size, low power consumption, and low cost are the primary goals, a compromise in choice of components and construction is re-

quired. In this respect a common laser with a spectral width in the tens of MHz used in conjunction with a ^{87}Rb cell containing a mixture of buffer gases at a pressure of 100 Torr can lead to frequency stability in the low $10^{-12}\,\tau^{-1/2}$. In all cases, as in the optical pumping with a spectral lamp approach, care needs to be taken in using an interrogation oscillator, that is quartz oscillator and synthesizer, having noise spectrum characteristics at the second harmonic of the modulating frequency that are compatible with the frequency stability desired.

ACKNOWLEDGEMENTS The authors wish to thank J.C. Camparo for his constructive comments on the manuscript.

Appendices

A Dynamics of radiation absorption in a cell under IOP

A.1 *Optical power absorbed in a Rb vapor cell*

In the evaluation of the optical power or optical flux absorbed in a resonant Rb vapor, authors use various expressions connecting the light intensity to internal parameters of the atomic ensemble. This annex reviews these different expressions and relate them to each other.

The power absorbed over a distance z is given by

$$P_{\text{abs}} = \int_z \boldsymbol{E}\cdot\frac{\mathrm{d}\boldsymbol{P}}{\mathrm{d}t}\,\mathrm{d}z\,, \tag{A.1}$$

where E is the electric field and P is the electric polarization of the atomic ensemble given by [19]

$$\boldsymbol{P}(z,t) = n\,\mathrm{Tr}\,(\varrho\boldsymbol{d})\,. \tag{A.2}$$

Here n is the Rb density, ϱ is the density matrix of the ensemble, d is the quantum mechanical operator for the electric dipole moment expressed as a matrix, and Tr means "take the trace of the resulting matrix multiplication". We assume that the laser is tuned to the optical transition μ to m. Straightforward matrix algebra, using the form of E given by (8) for the laser radiation, gives

$$\Delta P_{\text{abs}} = n(E_{0\text{L}}\omega_{\text{L}}\mathrm{Im}\delta_{\mu m}d_{m\mu})\,\mathrm{d}z\,. \tag{A.3}$$

Using (13) at equilibrium, and the definition of the Rabi frequency through (9), this may be written

$$\Delta P_{\text{abs}} = n\hbar\omega_{\text{L}}\Gamma^*\varrho_{mm}\,\mathrm{d}z\,, \tag{A.4}$$

which can also be written

$$\Delta P_{\text{abs}} = \Gamma_{\text{p}}n\hbar\omega_{\text{L}}\varrho_{\mu\mu}\,\mathrm{d}z\,. \tag{A.5}$$

It is often convenient to relate the pumping rate Γ_{p} to the absorption cross-section $\sigma(\nu)$ by means of the relation [12]

$$\Gamma_{\text{p}}(z) = \int_0^\infty \hat{I}(\nu,z)\sigma(\nu)\,\mathrm{d}\nu\,, \tag{A.6}$$

where $\hat{I}(\nu,z)$ is the flux of incident radiation in photons per second per m^2 per unit frequency interval. Simple algebraic considerations on the flux absorbed by the cell leads directly also to (A.5).

A.2 *Calculation in terms of the optical Rabi frequency*

The equation used in the text for absorption connects the Rabi frequency of the optical radiation to the coherence created by the incident optical radiation

$$\frac{\partial\Omega_{\text{L}\mu m}}{\partial z} = \alpha\mathrm{Im}\delta_{\mu m}\,, \tag{A.7}$$

where we have assumed that the laser frequency is tuned to the transition μ to m. This equation is equivalent to (A.4). This can be shown by means of the definition of Rabi frequency and, through (13) and the definition of the absorption coefficient α (22), (A.7) becomes

$$\varepsilon_0 cE_{\text{Lo}}\frac{\mathrm{d}}{\mathrm{d}z}E_{\text{Lo}} = n\hbar\omega_{\text{L}}\Gamma^*\varrho_{mm}\,. \tag{A.8}$$

Considerations on the energy flux traversing a cylinder of unit area and unit length gives power at the output of the cylinder as

$$P_{\text{out1}} = \frac{1}{2}\varepsilon_0 cE_{\text{Lo}}^2\,. \tag{A.9}$$

By direct substitution we finally obtain

$$\mathrm{d}P = n\hbar\omega_{\text{L}}\Gamma^*\varrho_{mm}\,\mathrm{d}z\,, \tag{A.10}$$

which is the same as (A.4).

B Coherence between levels μ' and m

The coherence $\delta_{\mu' m}$ is calculated from (21) as

$$\delta_{\mu' m} = -\mathrm{i}\frac{\Omega_{\text{L}\mu' m}/2}{\left(\frac{\Gamma^*}{2}+\mathrm{i}(\omega_{\text{L}}-\omega_{m\mu'})\right)}\varrho_{\mu'\mu'} + \mathrm{i}\frac{b/2}{\left(\frac{\Gamma^*}{2}+\mathrm{i}(\omega_{\text{L}}-\omega_{m\mu'})\right)}\varepsilon_{\mu m}\,, \tag{B.1}$$

where we have made $\varrho_{mm} \ll \varrho_{\mu'\mu'}$. Using (26) we obtain

$$\delta_{\mu' m} = -\mathrm{i}\frac{\Omega_{\text{L}\mu' m}/2}{\left(\frac{\Gamma^*}{2}+\mathrm{i}(\omega_{\text{L}}-\omega_{m\mu'})\right)}\varrho_{\mu'\mu'} - \frac{(b/2)^2}{\left(\frac{\Gamma^*}{2}+\mathrm{i}(\omega_{\text{L}}-\omega_{m\mu'})\right)\left(\frac{\Gamma^*}{2}+\mathrm{i}(\omega_{\text{L}}+\omega_{\text{M}}-\omega_{m\mu})\right)}\delta_{\mu' m} + \frac{(\Omega_{\text{L}\mu' m}/2)(b/2)}{\left(\frac{\Gamma^*}{2}+\mathrm{i}(\omega_{\text{L}}-\omega_{m\mu'})\right)\left(\frac{\Gamma^*}{2}+\mathrm{i}(\omega_{\text{L}}+\omega_{\text{M}}-\omega_{m\mu})\right)}\delta_{\mu\mu'}\,. \tag{B.2}$$

Following the discussion we made in connection to $\delta_{\mu m}$ and making the same approximations we obtain:

$$\delta_{\mu' m} = -\mathrm{i}\frac{\Omega_{\text{L}\mu' m}/2}{\left(\frac{\Gamma^*}{2}+\mathrm{i}(\omega_{\text{L}}-\omega_{m\mu'})\right)}\varrho_{\mu'\mu'}\,. \tag{B.3}$$

Due to the detuning of the laser relative to the transition $m \to \mu'$, we have $\omega_{\text{L}} - \omega_{m\mu'} = \omega_{\mu'\mu}$ and the coherence $\delta_{\mu' m}$ is very small. If the laser is tuned to the transition $m \to \mu'$, the situation is reversed and the analysis is similar to that done for the case when the laser is tuned to the transition $m \to \mu$.

REFERENCES

1 T.R. Carver, Proc. 11th Annual Frequency Control Symposium, 307 (1957)
2 M. Arditi, Proc. 12th Annual Frequency Control Symposium, 606 (1958)
3 M. Arditi, T.R. Carver, IRE National Convention Records, Pt **1**, 3 (1958)
4 A. Kastler, J. Phys. Radium **11**, 255 (1950)
5 P.L. Bender, E.C. Beaty, A.R. Chi, Phys. Rev. Lett. **1**, 311 (1958)
6 R.H. Dicke, Phys. Rev. **89**, 472 (1953)
7 H.G. Dehmelt, Phys. Rev. **105**, 1487 (1957)
8 M. Arditi, T.R. Carver, Phys. Rev. Lett. **109**, 1012 (1958)
9 E. Jechart, US Patent No 3,903,491 (1975)
10 J. Vanier, R. Kunski, P. Paulin, M. Têtu, N. Cyr, Can. J. Phys. **60**, 1396 (1982)
11 P. Davidovits, Appl. Phys. Lett. **5**, 15 (1964)
12 J. Vanier, Phys. Rev. **168**, 129 (1968)
13 N. Beverini, F. Strumia, Opt. Commun. **2**, 189 (1970)
14 G. Rovera, A. De Marchi, J. Vanier, IEEE Trans. Instrum. Meas. **IM-25**, 203 (1976)
15 G. Singh, P. DiLavore, C.O. Alley, IEEE J. Quantum Electron. **QE-7**, 196 (1971)
16 J.-L. Picqué, IEEE J. Quantum Electron. **QE-10**, 802 (1974)
17 J. Vanier, Appl. Phys. B **81**, 421 (2005)
18 J. Vanier, M. Levine, D. Janssen, M. Delaney, IEEE Trans. Instrum. Meas. **52**, 822 (2003)
19 J. Vanier, C. Audoin, *The Quantum Physics of Atomic Frequency Standards*, ed. by A. Hilger (Bristol, Philadelphia, 1989)
20 J. Vanier, M. Têtu, L.G. Bernier, IEEE Trans. Instrum. Meas. **IM-28**, 188 (1979)
21 J. Vanier, L.G. Bernier, IEEE Trans. Instrum. Meas. **IM-30**, 177 (1982)
22 W. Happer, Rev. Mod. Phys. **44**, 169 (1972)
23 J. Vanier, M. Levine, D. Janssen, M. Delaney, Phys. Rev. A **67**, 065 801 (2003)
24 U. Fano, Rev. Mod. Phys. **29**, 74 (1957)
25 J. Vanier, *Basic Theory of Lasers and Masers, A Density Matrix Approach* (Gordon & Breach, New York, 1971)
26 G. Mileti, Thèse, Université de Neuchâtel, Switzerland (1995), unpublished
27 A. Godone, F. Levi, S. Micalizio, J. Vanier, Eur. Phys. J. D **18**, 5 (2002)
28 M.O. Scully, M.S. Zubairy, *Quantum Optics* (Cambridge University Press, New York, 1999)
29 W. Happer, B.S. Mather, Phys. Rev. **163**, 12 (1967)
30 J. Vanier, Can. J. Phys. **47**, 1461 (1969)
31 P. Barrat, C. Cohen-Tannoudji, J. Phys. Radium **22**, 231, 443 (1961)
32 B.S. Mather, H. Tang, W. Happer, Phys. Rev. **171**, 11 (1968)
33 J.C. Camparo, R.P. Frueholz, Phys. Rev. A **31**, 1440 (1985)
34 G. Mileti, P. Thomann, Proc. 9th Euro. Forum on Time and Freq., 271 (1995)
35 J.C. Camparo, H.P. Frueholz, C.H. Volk, Phys. Rev. A **27**, 1914 (1983)
36 P.J. Chantry, B.R. McAvoy, J.M. Zomp, I. Liberman, Proc. IEEE Int. Freq. Control Symp. 114 (1992)
37 M. Hashimoto, M. Ohtsu, H. Furuta, Proc. 41st An. Freq. Control Symp. 25 (1987)
38 I. Matsuda, S. Yamaguchi, M. Suzuki, IEEE J. Quantum Electron. **QE-26**, 9 (1990)
39 L.L. Lewis, M. Feldman, Proc. 35th Ann. Freq. Control Symp. 612 (1981)
40 J.C. Camparo, R.P. Frueholz, Phys. Rev. A **31**, 1440 (1985)
41 J.C. Camparo, C.M. Klimcak, S.J. Herbulock, IEEE Trans. Instrum. Meas. **54**, 1873 (2005)
42 Y. Saburi, Y. Koga, S. Kinugawa, T. Imamura, H. Suga, Y. Ohuchi, IEEE Electron. Lett. **30**, 633 (1994)
43 M. Hashimoto, M. Ohtsu, IEEE J. Quantum Electron. **QE-23**, 446 (1987)
44 M. Hashimoto, M. Ohtsu, IEEE Trans. Instrum. Meas. **39**, 458 (1990)
45 M. Ohtsu, M. Hashimoto, O. Hidetaka, Proc. 39th Ann. Freq. Control Symp., 43 (1985)
46 P.J. Chantry, I.I. Liberman, W.R. Verbanets, C.F. Petronio, R.F. Cather, W.D. Partlow, Proc. IEEE Int. Freq. Control Symp. 1002 (1996)
47 G. Mileti, J.Q. Deng, F. Walls, D.A. Jennings, R.E. Drullinger, IEEE J. Quantum Electron. **QE-34**, 233 (1998)
48 Y. Ohuchi, H. Suga, T. Suzuki, M. Uchino, K. Takahei, M. Tsuda, Y. Saburi, Proc. IEEE Int. Freq. Control Symp., 651 (2000)
49 C. Afolderbach, G. Mileti, Proc. 35th Precise Time and Time Interval (PTTI) Meeting, 489 (2003)
50 J.C. Camparo, J.G. Coffer, Phys. Rev. A **59**, 728 (1999)
51 N.D. Bhaskar, Proc. Int. Freq. Control Symp. 87 (1993) and IEEE Trans. Ultrasonics Ferroelectr. Frequency Control **42**, 15 (1995)
52 G. Missout, J. Vanier, IEEE Trans. Instrum. Meas. **24**, 180 (1975)
53 J. Vanier, R. Kunski, N. Cyr, J.Y. Savard, M. Têtu, J. Appl. Phys. **53**, 5387 (1982)
54 Y. Ohuchi, H. Suga, T. Suzuki, M. Uchino, K. Takahei, M. Tsuda, Y. Saburi, Proc. IEEE Int. Freq. Control Symp., 651 (2000)
55 C. Affolderbach, F. Droz, G. Mileti, IEEE Trans. Instrum. Meas. **55**, 429 (2006)
56 J.C. Camparo, Proc. 50th IEEE Int. Freq. Control Symp., 988 (1996)
57 J. Camparo, J. Coffer, J. Townsend, J. Opt. Soc. Am. B **22**, 529 (2005)
58 M. Hashimoto, M. Ohtsu, J. Opt. Soc. Am. B **6**, 1777 (1989)
59 M. Arditi, J.-L. Picqué, J. Phys. B **8**, L331 (1975)
60 I. Matsuda, S. Yamaguchi, M. Suzuki, IEEE J. Quantum Electron. **QE-26**, 9 (1990)
61 S. Yamagushi, I. Matsuda, M. Suzuki, IEEE J. Quantum Electron. **QE-28**, 2551 (1992)
62 J. Deng, J. Liu, S. An, Y. Tan, X. Zhu, IEEE Trans. Instrum. Meas. **43**, 549 (1994)
63 G. Mileti, J.Q. Deng, F. Walls, J.P. Low, R.E. Drullinger, Proc. IEEE Int. Freq. Control Symp., 1066 (1996)
64 F. Levi, C. Novero, A. Godone, G. Brida, IEEE Trans. Instrum. Meas. **46**, 126 (1997)
65 C. Affolderbach, G. Mileti, D. Slavov, C. Andreeva, S. Cartaleva, Proc. 18th Eur. Frequency and Time Forum, 084 (2004)
66 F. Levi, Thesis, Politecnico di Torino, Italy (1995)
67 J.C. Camparo, J.G. Coffer, J.J. Townsend, Proc. IEEE Int. Freq. Control Symp., 134 (2004)
68 C. Affolderbach, G. Mileti, C. Andreeva, D. Slavov, T. Karaulanov, S. Cataleva, Proc. IEEE Int. Freq. Control Symp. jointly with 17th European Frequency and Time Forum, 27 (2003)
69 C. Affolderbach, C. Andreeva, S. Cartaleva, T. Karaulanov, G. Mileti, D. Slavov, Appl. Phys. B **80**, 841 (2005)
70 F. Levi, A. Godone, J. Vanier, IEEE Trans. Instrum. Meas. **47**, 466 (2000)
71 J. Deng, Proc. IEEE Int. Freq. Control Symp., 659–663 (2000)
72 J. Camparo, S.B. Delcamp, Opt. Commun. **120**, 257 (1995)
73 J. Camparo, Proc. 50th IEEE Int. Freq. Control Symp., 988 (1996)
74 T.C. English, E. Jechart, T.M. Kwon, Proc. 10th PTTI, p. 147 (1978)
75 E.I. Alekseyev, Y.N. Bazarov, G.I. Telegin, Radio Eng. Electron. Phys. **20**, 73 (1975)
76 M. Arditi, T.R. Carver, IEEE Trans. Instrum. Meas. **13**, 146 (1964)
77 A. Godone, S. Micalizio, F. Levi, Phys. Rev. A **70**, 023 409 (2004)
78 A. Godone, S. Micalizio, F. Levi, C. Calosso, Phys. Rev. A **74**, 043 401 (2006)
79 A. Risley, G. Busca, Proc. 32nd Frequency Control Symposium, 506 (1978)
80 S. Micalizio, A. Godone, F. Levi, J. Vanier, Phys. Rev. A **73**, 033 414 (2006)
81 G. Mileti, I. Rüedi, M. Schweda, Proc. 6th Eur. Frequency and Time Forum, 515 (1992)
82 A. Risley, S. Jarvis, J. Vanier, J. Appl. Phys. **51**, 4571 (1980)
83 J.C. Camparo, R.P. Frueholz, IEEE Trans. Ultrasonics Ferroelectr. Frequency Control **36**, 185 (1989)
84 E.B. Sarozi, W.A. Sarozi, W.A. Johnson, S.K. Karuza, Proc. 23rd An. Prec. Time and Time Interval (PTTI) App. Plan. Meet. 229 (1992)
85 J.C. Camparo, Phys. Rev. Lett. **80**, 222 (1998)
86 J.C. Camparo, Phys. Rev. A **62**, 013 812 (2000)
87 X. Huang, B. Xia, D. Zhong, S. An, X. Zhu, G. Mei, Proc. IEEE Int. Freq. Control Symp., 105 (2001)
88 J.G. Coffer, B. Sickmiller, J.C. Camparo, IEEE Trans. Ultras. Ferooel. Freq. Cont. **51**, 129 (2004)
89 D. Halford, Proc. of the Frequency standards and metrology seminar, 413 unpublished, Laval University Quebec, Canada (1971)
90 C. Mandache, Rapport de stage, Mairie de Paris, France (2006), unpublished
91 I. Joindot, J. Phys. III France **2**, 1591 (1992)
92 N. Sagna, C. Mandache, P. Thomann, Proc. 6th European Frequency and Time Forum, 521 (1992)
93 J.G. Coffer, J.C. Camparo, Proc. IEEE Int. Freq. Control Symp., 52

(1998)
94 H. Tsuchida, T. Tako, Japan. J. Appl. Phys. **22**, 1152 (1983)
95 M. de Labachelerie, C. Latrasse, P. Kemssu, P. Cerez, J. Phys. III France **2**, 1557 (1992)
96 M. Ohtsu, K. Nakagawa, M. Kourogi, W. Wang, J. Appl. Phys. **73**, R1 (1993)
97 L. Goldberg, H.F. Taylor, A. Dandridge, J.F. Weller, R.O. Miles, IEEE J. Quantum Electron. **QE-18**, 555 (1982)
98 T. Kanada, K. Nawata, Opt. Commun. **31**, 81 (1979)
99 S. Saito, O. Nilsson, Y. Yamamoto, IEEE J. Quantum Electron. **QE-18**, 961 (1982)
100 M. de Labachellerie, P. Cerez, Opt. Commun. **55**, 174 (1985)
101 B. Dahmani, L. Hollberg, R. Drullinger, Opt. Lett. **12**, 876 (1987)
102 P. Laurent, A. Clairon, C. Bréant, IEEE J. Quantum Electron. **QE-25**, 1131 (1989)
103 H. Li, H.R. Telle, IEEE J. Quantum Electron. **QE-25**, 257 (1989)
104 M. Ohtsu, M. Hashimoto, O. Hidetaka, Proc. 39th Ann. Freq. Control Symp., 43 (1985)
105 M. Kozuma, M. Kourogi, M. Ohtsu, Appl. Phys. Lett. **61**, 1895 (1992)
106 M. de Labachelerie, K. Diomande, N. Dimarcq, Proc. 2nd European Frequency and Time Forum, Neuchâtel, 547 (1988)
107 M.W. Fleming, A. Mooradian, IEEE J. Quantum Electron. **QE-17**, 44 (1981)
108 H. Tsuchida, M. Ohtsu, T. Tako, Japan. J. Appl. Phys. **21**, L561 (1982)
109 G.P. Barwood, P. Gill, W.R.C. Rowley, J. Phys. E **21**, 966 (1988)
110 G.P. Barwood, P. Gill, W.R.C. Rowley, Appl. Phys. B **53**, 142 (1991)
111 N. Beverini, E. Maccioni, P. Marsili, A. Ruffini, F. Sorrentino, Appl. Phys. B **73**, 133 (2001)
112 C. Afolderbach, G. Mileti, Proc. IEEE Int. Freq. Cont. Symp. jointly with 17th Eur. Frequency and Time Forum, 109 (2003)
113 C. Affolderbach, G. Mileti, D. Slavov, C. Andreeva, S. Cartaleva, Proc. 18th Eur. Frequency and Time Forum, 84 (2004)
114 C. Affolderbach, F. Droz, G. Mileti, Rev. Sci. Instrum. **76**, 073 108 (2005)
115 J.C. Camparo, W.F. Buell, Proc. IEEE Int. Freq. Control Symp., 253 (1997)
116 J.G. Coffer, J.C. Camparo, Proc. IEEE Int. Freq. Control Symp., 52 (1998)
117 J.C. Camparo, J. Opt. Soc. Am. B **15**, 1177 (1998)
118 J.C. Camparo, J.G. Coffer, Phys. Rev. A **59**, 728 (1999)
119 J.C. Camparo, Report No TR-96(8555)-2 25430, The Aerospace Corporation, El Segundo, CA 90245-4691, 10 March 2000
120 J.G. Coffer, M. Anderson, J.C. Camparo, Phys. Rev. A **65**, 033 807 (2002)
121 G. Mileti, J.Q. Deng, F. Walls, D.A. Jennings, R.E. Drullinger, IEEE J. Quantum Electron. **QE-34**, 233 (1998)
122 G. Kramer, CPEM 1974 Digest, IEEE Conf. Pub. No 113, unpublished
123 C. Audoin, V. Candelier, N. Dimarcq, IEEE Trans. Instrum. Meas. **40**, 121 (1991)
124 C. Szekely, F. Walls, J.P. Lowe, R.E. Drullinger, A. Novick, IEEE Trans. Ultrasonics Ferroelectr. Frequency Control **41**, 518 (1994)
125 J.Q. Deng, G. Mileti, D.A. Jennings, R.E. Drullinger, F. Walls, Proc. IEEE Int. Freq. Control Symp., 438 (1997)
126 J.Q. Deng, A. De Marchi, F.L. Walls, R.E. Drullinger, IEEE Int. Freq. Cont. Symp., 95 (1998)
127 A. De Marchi, L. Lo Presti, G.D. Rovera, IEEE Int. Freq. Cont. Symp., 104 (1998)
128 M. Ortalano, N. Beverini, A. De Marchi, IEEE Trans. Ultrasonics Ferroelectr. Frequency Control **47**, 471 (2000)
129 N. Beverini, M. Ortalano, G.A. Costanzo, A. De Marchi, E. Maccioni, P. Marsili, A. Ruffini, F. Periale, V. Barychev, Laser Phys. **11**, 1110 (2001)
130 J. Camparo, IEEE Trans. Ultrasonics Ferroelectr. Frequency Control **52**, 1075 (2005)
131 V. Shaw, V. Gerginov, P.D.D. Schwindt, S. Knappe, L. Hollberg, J. Kitching, Appl. Phys. Lett. **89**, 151 124 (2006)
132 P. Davidovits, R. Novick, Proc. IEEE **54**, 155 (1966)
133 M. Têtu, G. Busca, J. Vanier, IEEE Trans. Instrum. Meas. **IM-22**, 250 (1973)
134 G. Busca, R. Brousseau, J. Vanier, IEEE Trans. Instrum. Meas. **IM-24**, 291 (1975)
135 A. Michaud, P. Tremblay, M. Têtu, IEEE Trans. Instrum. Meas. **40**, 170 (1991)
136 A. Michaud, P. Tremblay, M. Têtu, IEEE CPEM Digest, 155, unpublished (1990)
137 J. Deng, J. Liu, S. An, Y. Tan, X. Zhu, IEEE Trans. Instrum. Meas. **43**, 549 (1994)
138 N.F. Ramsey, *Molecular Beams* (Clarendon Press, Oxford, 1956)
139 M. Arditi, T.R. Carver, IEEE Trans. Instrum. Meas. **13**, 146 (1964)
140 A. Godone, S. Micalizio, C.E. Calosso, F. Levi, IEEE Trans. Ultrasonics Ferroelectr. Frequency Control **53**, 525 (2006)
141 J. Vanier, C. Audoin, Metrologia **42**, S31 (2005)
142 A. Godone, S. Micalizio, F. Levi, C.E. Calosso, Phys. Rev. A **7**, 014 340 (2006)
143 H. Robinson, Appl. Phys. Lett. **40**, 771 773 (1982)
144 M.A. Bouchiat, *Etude par pompage optique de la relaxation d'atomes de rubidium* (Publications scientifiques et techniques du Ministère de l'air, Paris, 1965)
145 J. Vanier, J.F. Simard, J.S. Boulanger, Phys. Rev. A **9**, 1031 (1974)
146 J. Vanier, R. Kunski, A. Brisson, P. Paulin, J. Phys. C **8**, **42**, 139 (1981)
147 Y. Xiao, I. Novikova, D.F. Phillips, R.L. Walsworth, Phys. Rev. Lett. **96**, 043 601 (2006)